



Article

Design, Synthesis and Biological Evaluation of 6-(Imidazo[1,2-a]pyridin-6-yl)quinazoline Derivatives as Anticancer Agents via PI3K α Inhibition

Mei Li ^{1,2,†}, Daoping Wang ^{1,2,†}, Qing Li ^{1,2}, Fang Luo ^{1,2}, Ting Zhong ^{1,2}, Hongshan Wu ^{1,2}, Liang Xiong ^{1,2}, Meitao Yuan ^{1,2}, Mingzhi Su ^{1,2} and Yanhua Fan ^{1,2,*}

¹ State Key Laboratory for Functions and Applications of Medicinal Plants, Guizhou Medical University, Guiyang 550014, China

² The Key Laboratory of Chemistry for Natural Products of Guizhou Province and Chinese Academy of Sciences, Guiyang 550014, China

* Correspondence: yhfan@gmc.edu.cn

† These authors contributed equally to this work.

Abstract: Aberrant expression of the phosphatidylinositol 3-kinase (PI3K) signalling pathway is often associated with tumourigenesis, progression and poor prognosis. Hence, PI3K inhibitors have attracted significant interest for the treatment of cancer. In this study, a series of new 6-(imidazo[1,2-a]pyridin-6-yl)quinazoline derivatives were designed, synthesized and characterized by ¹H NMR, ¹³C NMR and HRMS spectra analyses. In the in vitro anticancer assay, most of the synthetic compounds showed submicromolar inhibitory activity against various tumour cell lines, among which **13k** is the most potent compound with IC₅₀ values ranging from 0.09 μ M to 0.43 μ M against all the tested cell lines. Moreover, **13k** induced cell cycle arrest at G2/M phase and cell apoptosis of HCC827 cells by inhibition of PI3K α with an IC₅₀ value of 1.94 nM. These results suggested that compound **13k** might serve as a lead compound for the development of PI3K α inhibitor.

Keywords: cell cycle arrest; cell apoptosis; PI3K α inhibitor; quinazoline; imidazo[1,2-a]pyridine



Citation: Li, M.; Wang, D.; Li, Q.; Luo, F.; Zhong, T.; Wu, H.; Xiong, L.; Yuan, M.; Su, M.; Fan, Y. Design, Synthesis and Biological Evaluation of 6-(Imidazo[1,2-a]pyridin-6-yl)quinazoline Derivatives as Anticancer Agents via PI3K α Inhibition. *Int. J. Mol. Sci.* **2023**, *24*, 6851. <https://doi.org/10.3390/ijms24076851>

Academic Editor: Nam Deuk Kim

Received: 15 February 2023

Revised: 30 March 2023

Accepted: 3 April 2023

Published: 6 April 2023



Copyright: © 2023 by the authors. Licensee MDPI, Basel, Switzerland. This article is an open access article distributed under the terms and conditions of the Creative Commons Attribution (CC BY) license (<https://creativecommons.org/licenses/by/4.0/>).

1. Introduction

Phosphatidylinositol 3-kinase (PI3K) is a lipid kinase that plays a key regulatory role in various cellular physiological processes including cell growth, proliferation, survival and metabolism [1,2]. Akt (protein kinase B, PKB) is a serine/threonine kinase and participates in the key role of the PI3K signalling pathway. Research shows that mutations and abnormal activation of the PI3K-AKT pathway are often identified as one of the major factors resulted in tumourigenesis, progression and poor prognosis [3–5]. PI3K is usually divided into three categories (classes I, II and III) [6]. PI3K α belongs to class I, which mainly consists of a regulatory subunit (p85) and a catalytic subunit (p110) [7]. The mutation of PIK3CA, the encoding gene of PI3K α , is one of the most common mutations in tumours and would result in the under-expression or absence of PTEN (phosphatase and tensin homolog) and hyperactivation of PI3K downstream signalling pathways [8,9]. Due to the critical roles of PI3K signalling pathway in tumour occurrence, development and drug resistance, inhibitors targeting PI3K have attracted widespread attention [10,11]. Currently, dozens of subtype-selective and pan-PI3K inhibitors are in various stages of clinical studies for the treatment of human malignancies, yet the discovery of additional lead compounds for novel PI3K α inhibitors with better efficacy and less toxic side effects remains an urgent therapeutic need [12–14].

Quinazolines are the major compounds in the aromatic backbone of nitrogen-containing heterocyclic compounds with a wide range of biological activities such as anti-inflammatory, antimicrobial, antimalarial and antitumour [15–17]. In particular, many drugs containing 4-aminoquinazoline structures have been reported to exhibit prominent antitumour

activity through various mechanisms [18–21]. In recent years, it has been shown that 4-aminoquinazoline derivatives show good antitumour activity by inhibiting PI3K α [22]. This shows that 4-aminoquinazolines are an important class of molecular scaffold that can be used for the development of antitumour drugs.

In a previous study, we designed and synthesised a series of 4-aminoquinazoline derivatives and obtained a compound **6b** as a PI3K α inhibitor [23]. Based on the previous structure activity relationships (SAR) analysis and pharmacophore fusion strategy, structure modification of **6b** was performed to further improve the activity. According to the SAR analysis, 4-aminoquinazoline derivative moiety is the main critical pharmacophore of **6b** for its PI3K α inhibitory activity. Therefore, this moiety was retained as the basic scaffold for our target compound. Since imidazo[1,2-a]pyridine, the key pharmacodynamic group of PI3K α inhibitors TAK-117 and HS-173, is an important class of nitrogen-containing fused heterocyclics compounds that can effectively inhibit the growth of cancer cells, it was introduced to the position 6 of 4-aminoquinazoline [24–28]. Herein, a series of 6-(imidazo[1,2-a]pyridin-6-yl)quinazoline derivatives were designed and synthesized (Figure 1), and biological evaluation was performed to verify their PI3K α inhibitory activities and antitumour effects.

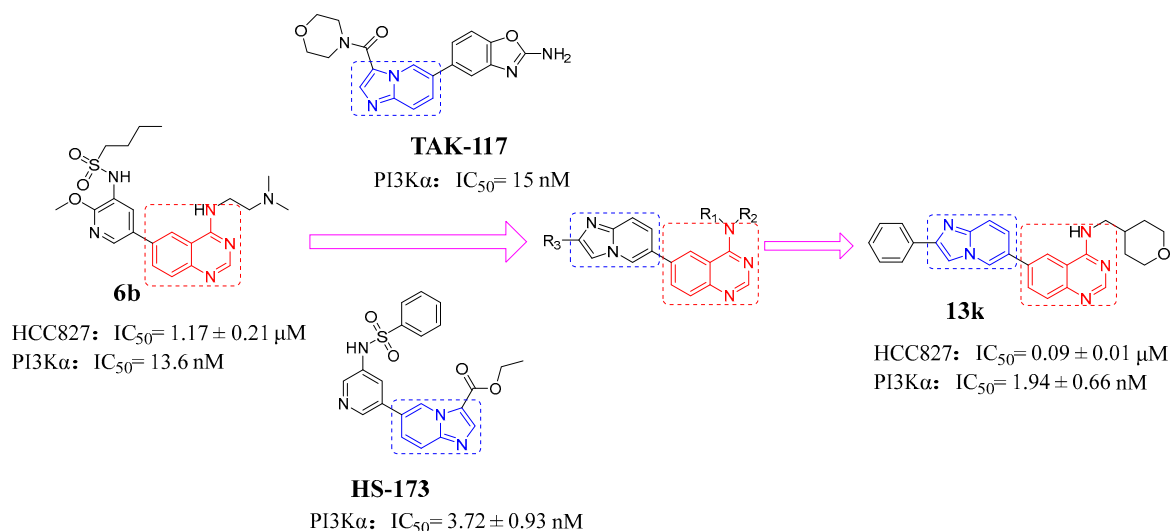
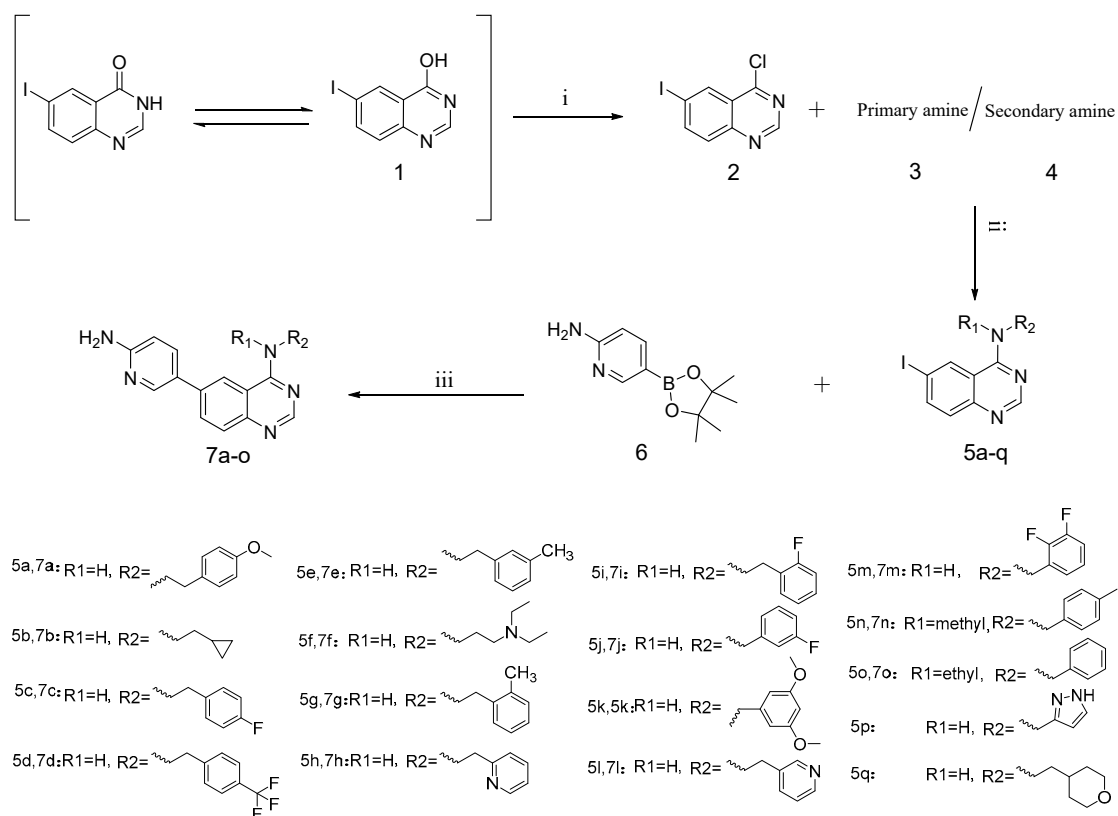


Figure 1. Design strategies for target compounds.

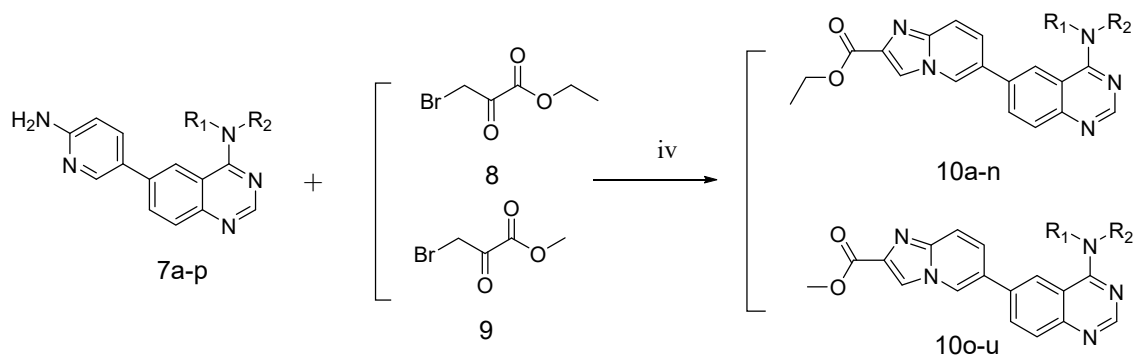
2. Results and Discussion

2.1. Chemistry

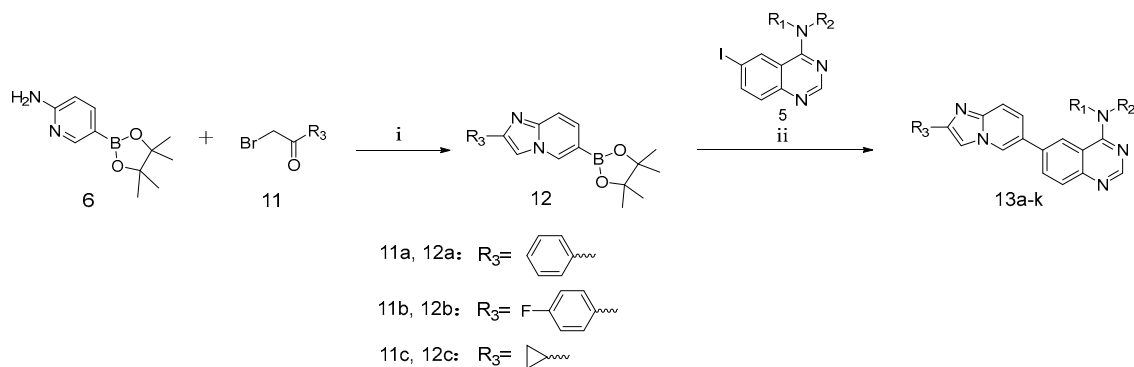
The synthetic route for intermediates **7a–o** of target products **10a–u** is shown in Scheme 1. A purchased raw material, 6-iodoquinazoline 4-3(H)-one was chlorinated in POCl₃ in the presence of DIPEA to give intermediate **2**. Intermediates **5a–q** were obtained by nucleophilic substitution reaction with primary or secondary amines, which subsequently reacted with 2-aminopyridine-5-boronic pinacol ester acid by Suzuki–Miyaura cross-coupling reaction to give intermediates **7a–o**. Intermediates **7a–o** were cyclized with methyl bromopyruvate or ethyl bromopyruvate to give the target products **10a–u**, as shown in Scheme 2. To improve the inhibitory activities of the target compounds, we performed further optimization of the substituents. Unfortunately, when the ester side chain was replaced with a cycloalkane, we failed to yield our target products by Scheme 2, so we opted for an alternative synthetic route. As shown in Scheme 3, intermediate **6** reacted with compound **11** to afford compound **12**, which was coupled with intermediates **5** to give our target products **13a–k** by Suzuki–Miyaura cross-coupling reaction. In this thesis, we introduced different substituents at the C⁶ and C⁴ positions of the 4-aminoquinazoline backbone and synthesised various ester and amines to further explore their possible structure–activity relationship (SAR), and all compounds are shown in Table 1.



Scheme 1. Preparation of 7a–7p reagents and conditions: (i) DIPEA, POCl₃, Toluene, 80 °C, 4 h; (ii) isopropanol, 60 °C, 2 h; (iii) K₂CO₃, Pd(dppf)Cl₂, 1,4-dioxacyclohexane/H₂O, 100 °C, 5 h.



Scheme 2. Preparation of 10a–10u reagents and conditions: (iv) NaHCO₃, EtOH, 80 °C, 4 h.



Scheme 3. Preparation of 13a–13k reagents and conditions: (i) NaHCO₃, EtOH, 80 °C, 4 h; (ii) K₂CO₃, Pd(dppf)Cl₂, 1,4-dioxacyclohexane/H₂O, 100 °C, 5 h.

Table 1. Anti-tumour activity of different cell lines (IC₅₀, μM)^a.

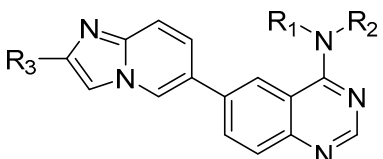
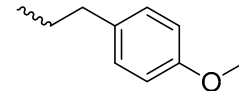
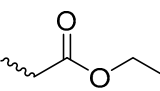
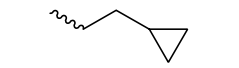
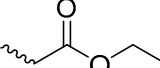
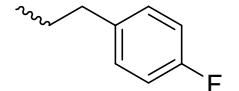
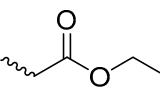
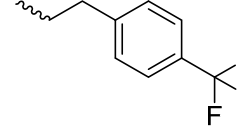
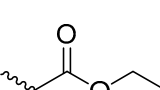
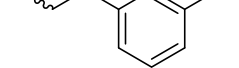
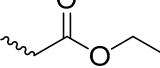
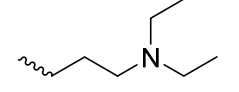
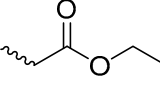
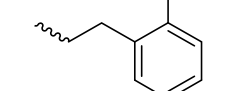
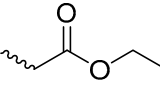
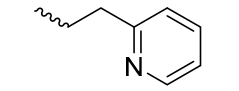
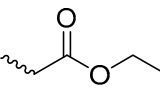
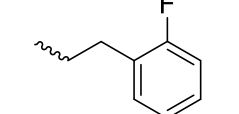
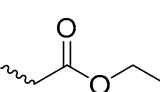
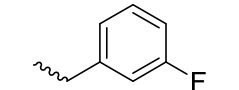
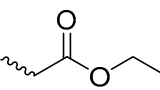
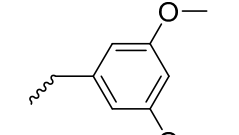
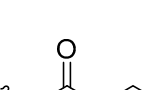
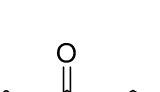
								
Comp.	R ₁	R ₂	R ₃	HCC827	A549	SH-SY5Y	HEL	MCF-7
10a	H			>10	>10	>10	>10	>10
10b	H			0.59 ± 0.18	1.16 ± 0.27	1.89 ± 0.60	0.82 ± 0.25	2.86 ± 0.80
10c	H			>10	>10	>10	>10	>10
10d	H			>10	>10	>10	>10	>10
10e	H			>10	>10	>10	>10	>10
10f	H			>10	>10	>10	>10	>10
10g	H			>10	>10	>10	>10	>10
10h	H			7.26 ± 1.35	7.30 ± 1.97	7.06 ± 0.16	5.37 ± 1.07	>10
10i	H			>10	>10	>10	9.51 ± 1.60	>10
10j	H			1.76 ± 0.77	8.49 ± 1.97	>10	6.87 ± 3.80	>10
10k	H			>10	>10	>10	>10	>10
10l	H			1.04 ± 0.79	2.01 ± 0.88	1.20 ± 0.35	2.90 ± 0.51	7.47 ± 1.31

Table 1. Cont.

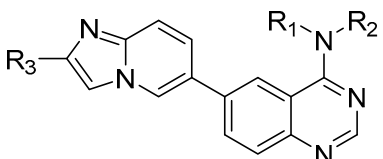
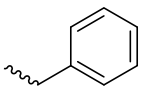
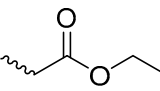
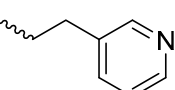
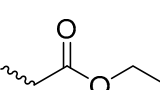
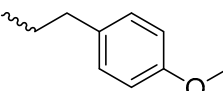
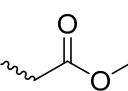
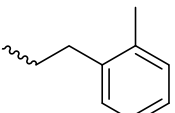
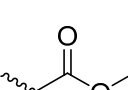
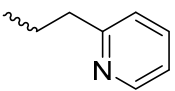
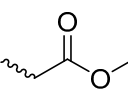
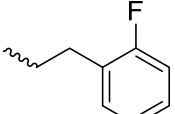
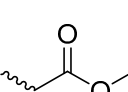
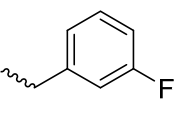
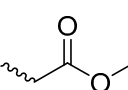
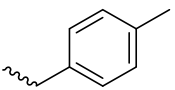
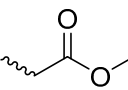
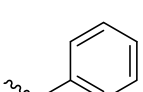
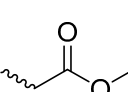
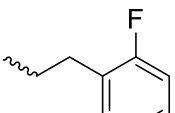
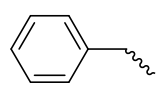
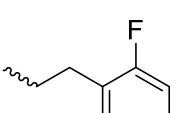
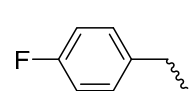
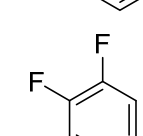
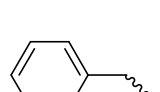
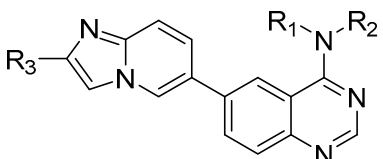
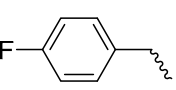
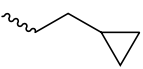
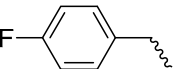
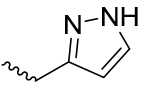
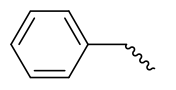
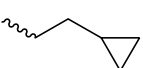
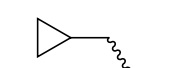
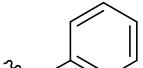
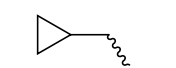
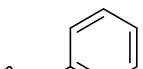
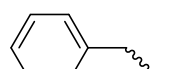
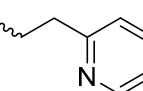
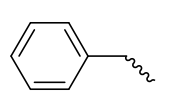
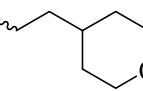
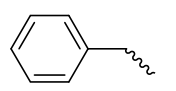
								
Comp.	R ₁	R ₂	R ₃	HCC827	A549	SH-SY5Y	HEL	MCF-7
10m				>10	>10	9.26 ± 1.54	>10	>10
10n	H			>10	>10	>10	>10	>10
10o	H			>10	>10	>10	>10	>10
10p	H			>10	>10	>10	>10	>10
10q	H			1.83 ± 0.70	4.22 ± 0.23	4.27 ± 0.66	2.10 ± 0.66	4.94 ± 0.54
10r	H			5.21 ± 2.40	3.31 ± 2.13	4.64 ± 0.71	5.49 ± 0.94	8.15 ± 1.10
10s	H			0.91 ± 0.21	5.71 ± 3.99	>10	2.91 ± 1.02	5.52 ± 1.02
10t				>10	>10	>10	7.22 ± 2.44	>10
10u				>10	>10	>10	>10	>10
13a	H			0.94 ± 0.14	1.18 ± 0.45	3.24 ± 1.76	0.55 ± 0.25	2.54 ± 0.57
13b	H			4.14 ± 0.65	3.11 ± 0.20	4.38 ± 1.11	2.10 ± 0.41	4.47 ± 0.39
13c	H			0.99 ± 0.23	1.78 ± 0.96	1.91 ± 0.61	1.45 ± 0.73	4.72 ± 0.72

Table 1. Cont.

Comp.				HCC827	A549	SH-SY5Y	HEL	MCF-7
	R ₁	R ₂	R ₃					
13d	H			7.45 ± 1.36	>10	7.91 ± 1.84	7.11 ± 3.30	>10
13e	H			8.47 ± 0.76	4.60 ± 0.38	7.54 ± 1.06	7.58 ± 1.54	6.11 ± 1.90
13f	H			0.83 ± 0.13	2.08 ± 0.30	5.63 ± 1.50	1.65 ± 0.23	5.66 ± 2.64
13g	H			0.50 ± 0.27	1.18 ± 0.69	4.62 ± 1.23	1.40 ± 0.84	5.39 ± 1.76
13h				>10	>10	7.99 ± 2.54	5.08 ± 0.21	>10
13i				>10	>10	6.62 ± 1.05	>10	>10
13j	H			7.10 ± 1.83	1.23 ± 0.34	2.94 ± 0.77	0.83 ± 0.22	>10
13k	H			0.09 ± 0.01	0.18 ± 0.01	0.37 ± 0.08	0.19 ± 0.01	0.43 ± 0.04
HS-173				3.90 ± 0.34	5.91 ± 0.19	10.71 ± 1.92	5.24 ± 1.28	4.36 ± 0.90

^a IC₅₀ values are the mean of triplicate measurements.

2.2. Biological Evaluation

2.2.1. Antiproliferation Activity Assay

To test the antiproliferative activity of all target compounds, IC₅₀ values were measured by MTT assay on various cancer cell lines including HCC827 (human non-small cell lung cancer cells), A549 (human non-small cell lung cancer cells), SH-SY5Y (human neuroblastoma cells), HEL (human erythroid and leukocyte leukaemia cells) and MCF-7 (human breast cancer cells). As shown in Table 1, most of the compounds showed significant antiproliferative activity in all the test cancer cells. Notably, most of the active compounds were more sensitive to HCC827 cells. In addition to HCC827 cells, PI3K was also overexpressed in other tested cells [29–32]. As to the reasons for the different sensitivity of the compounds to these tested cells, we hypothesized it might be because the PI3K pathway is not as equally important in the survival and proliferation of these cells as it is in HCC827 cells. For example, when PI3K signalling pathway is inhibited in A549 cells, cells can still maintain cell survival and proliferation through Ras/MERK/ERK pathway [33], which hence leads to different inhibitory activities of PI3K inhibitors in these two cells. According to the data of the antiproliferative assay, we conclude the following structure activity relationship. (I) In general, the antiproliferative activity of the compounds significantly decreased when R₁ substituent group was an alkyl, suggesting that simultaneous alkylation of NH₂ at the 4-position of quinazolinone would impair the antiproliferative activity

of the target compounds. (II) When $R_3 = \text{COOCH}_3$, most of the compounds are more active than $R_3 = \text{COOC}_2\text{H}_5$, such as compounds **10q** and **10h**, **10r** and **10i**, and when $R_3 = \text{COOC}_2\text{H}_5$ and R_2 is pyridine, the ortho-nitrogen is more active than meta-nitrogen. (III) The activity of the compounds was generally increased when benzene was introduced into the R_3 , as in **13c** and **10l**, **13a** and **10r**, but a decrease in activity was found with the introduction of the electron withdrawing group F on the R_3 -substituted benzene, as in compounds **13a** and **13b**, **13c** and **13d**. Overall, compound **13k** showed the best antiproliferative activity against HCC827 cells with an IC_{50} value of $0.09 \mu\text{M}$, which could be attributed to the conventional hydrogen bond formed between the R_2 -substituted tetrahydropyran and residue Gln859 in the active site of the target proprotein. To evaluate the selectivity of **13k** on cancer cells, the cytotoxicity of **13k** on human normal cell MRC-5 (human embryonic lung fibroblasts) was determined. Compound **13k** showed much less antiproliferative activity against MRC-5 with an IC_{50} value of $1.98 \mu\text{M}$, which is more than 20-fold different from HCC827 cells (Table 2). Moreover, as shown in Figure 2, **13k** treatment time-dependently inhibited the proliferation of HCC827 cells. Taken together, we chose HCC827 cells to further explore the anticancer effects and mechanisms of **13k**.

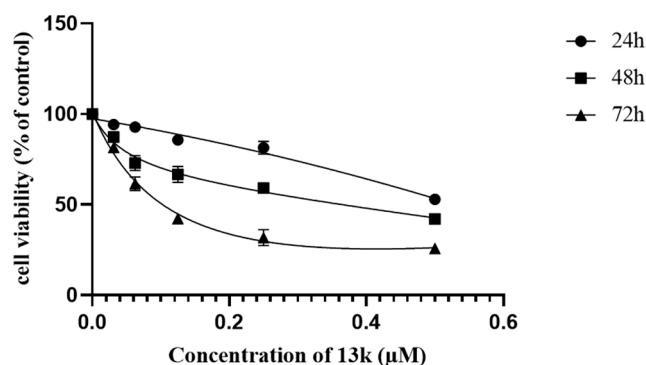


Figure 2. The time-dependent activity of **13k** on HCC827 cells. Cells were treated with **13k** (0.03 to $0.50 \mu\text{M}$) for 24 h to 72 h, and the survival rates were detected via MTT assay.

Table 2. Cytotoxicity of **13k** to normal human cells ($\text{IC}_{50} \mu\text{M}$)^a.

Cell	MRC-5
13k	1.98 ± 0.89

^a IC_{50} value is the mean of triplicate measurements.

2.2.2. Compound **13k** Inhibits PI3K α and Blocks the PI3K Pathway in HCC827 Cells

To evaluate the *in vitro* kinase inhibitory activity of **13k** against PI3K α , the kinase activity of PI3K α was tested using the ADP-GloTM Max Assay method. HS-173, a known PI3K α inhibitor, was used as a positive control. As shown in Table 3, **13k** significantly inhibited the kinase activity of PI3K α with an IC_{50} value of 1.94 nM . This suggests that compound **13k** is a potential PI3K α inhibitor.

Table 3. PI3K α kinase inhibition by **13k** ($\text{IC}_{50} \text{ nM}$)^a.

Compounds	PI3K α (IC_{50})
13k	1.94 ± 0.66
HS-173	3.72 ± 0.93

^a IC_{50} values are the mean of triplicate measurements.

Aberrant expression of PI3K signalling pathway is closely related to the process of tumourigenesis [34]. Lung cancer is the most lethal malignancy in the world, with non-small cell lung cancer (NSCLC) being the most commonly reported histological subtype [35]. According to reports, new oncogene changes have been discovered in NSCLC, including genetic changes in the PI3K pathway, and PIK3CA mutations in NSCLC may co-occur with

epidermal growth factor receptor (EGFR), Kirsten rat sarcoma viral oncogene homologue (KRAS) and anaplastic lymphoma kinase (ALK) mutations [36,37]. Therefore, we chose compound **13k** to investigate the mechanism of this compound in HCC827 cells. Since **13k** significantly inhibited PI3K α activity, we further verified the effects of **13k** on the PI3K/AKT pathway by Western blot. As shown in Figure 3, the phosphorylation level of PI3K was significantly reduced after **13k** treatment in a dose-dependent manner. The phosphorylation levels of its downstream proteins, AKT, mTOR and GSK3 β , were correspondingly reduced. The results confirmed the inhibitory effect of **13k** on PI3K pathway. The AKT/MAPK signalling pathway, downstream of PI3K, is considered a classical cancer signalling pathway and is involved in the development of many cancers [38–40]. Hence, PI3K inhibitors usually also affect the activation of three major categories of MAPK including ERK, JNK and p38 [41]. As shown in Figure 4, the p-JNK/JNK and p-p38/p38 values of HCC827 cells after **13k** treatment were significantly higher than those of the control group, indicating that **13k** can regulate the MAPK pathway through AKT.

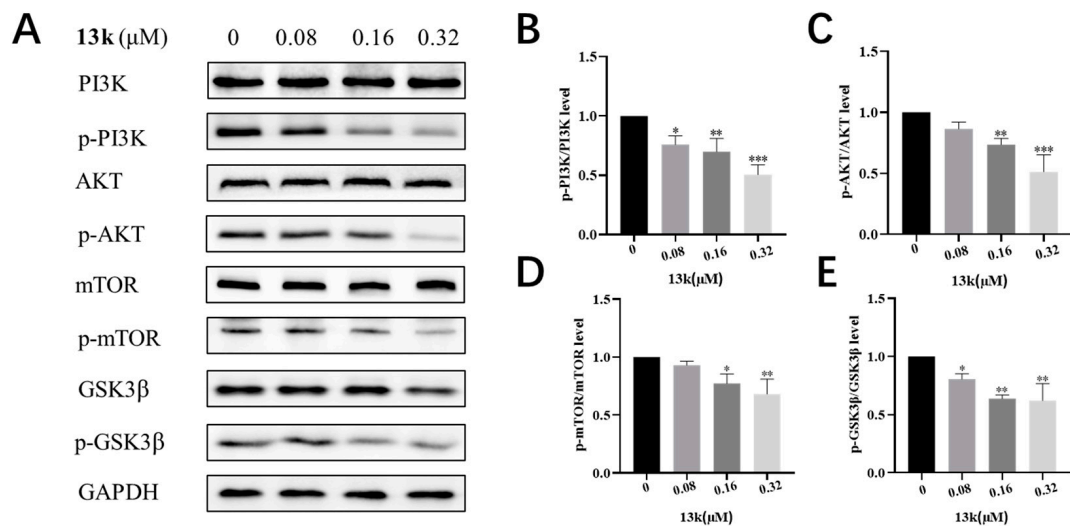


Figure 3. Compound **13k** inhibited the expression of PI3K and its downstream related proteins (A–E). Expression of PI3K-related proteins was analysed by immunoblotting after treatment of cells with different concentrations of compound **13k** (0, 0.08, 0.16 and 0.32 μ M) for 48 h. Expression of the associated proteins was analysed using Image J. Each bar data are expressed as mean \pm SD from three parallel experiments (* $p < 0.05$, ** $p < 0.01$, *** $p < 0.001$ vs. control).

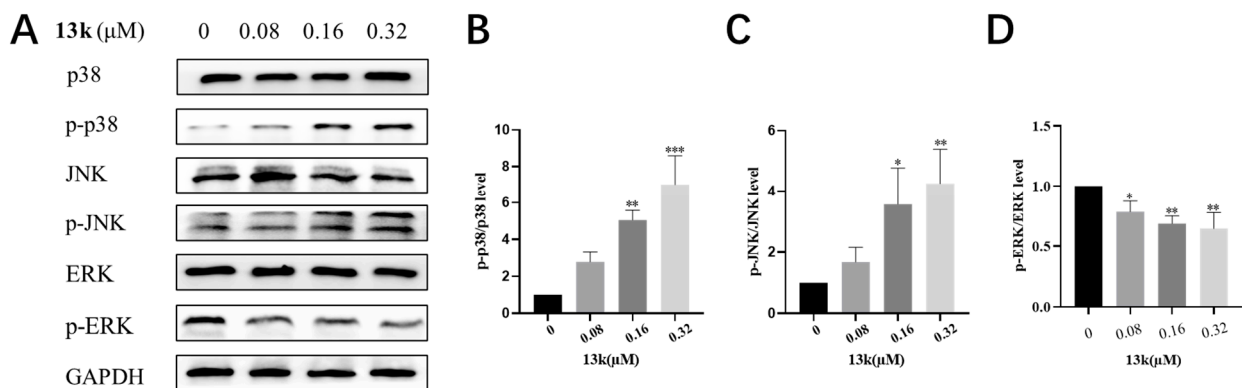


Figure 4. Effect of compound **13k** on the MAPK signalling pathway (A–D). Expression of related proteins was analysed by immunoblotting after treatment of cells with different concentrations of compound **13k** (0, 0.08, 0.16 and 0.32 μ M) for 48 h. Expression of the associated proteins was analysed using Image J. Each bar Data are expressed as mean \pm SD from three parallel experiments (* $p < 0.05$, ** $p < 0.01$, *** $p < 0.001$ vs. control).

2.2.3. Molecular Docking Study of Compound **13k**

Molecular docking simulations were performed to investigate the binding mode between **13k** and its target protein PI3K α (PDB code: 4ZOP). Similar to the binding mode of PI3K α inhibitor previously discovered, **13k** formed two conventional hydrogen bonds with the residues Lys802 and Gln859 as well as hydrophobic interactions including van der Waals, pi-pi T-shaped and pi-sulfur interactions in the active site of PI3K α . As shown in Figure 5, the benzene ring of compound **13k** also formed a pi-alkyl interaction with Leu807 disability. The results indicated that **13k** could engage the ATP-binding pocket of PI3K α . In addition, **13k** also formed similar hydrophobic interactions with residues in the acetyl-lysine binding sites.

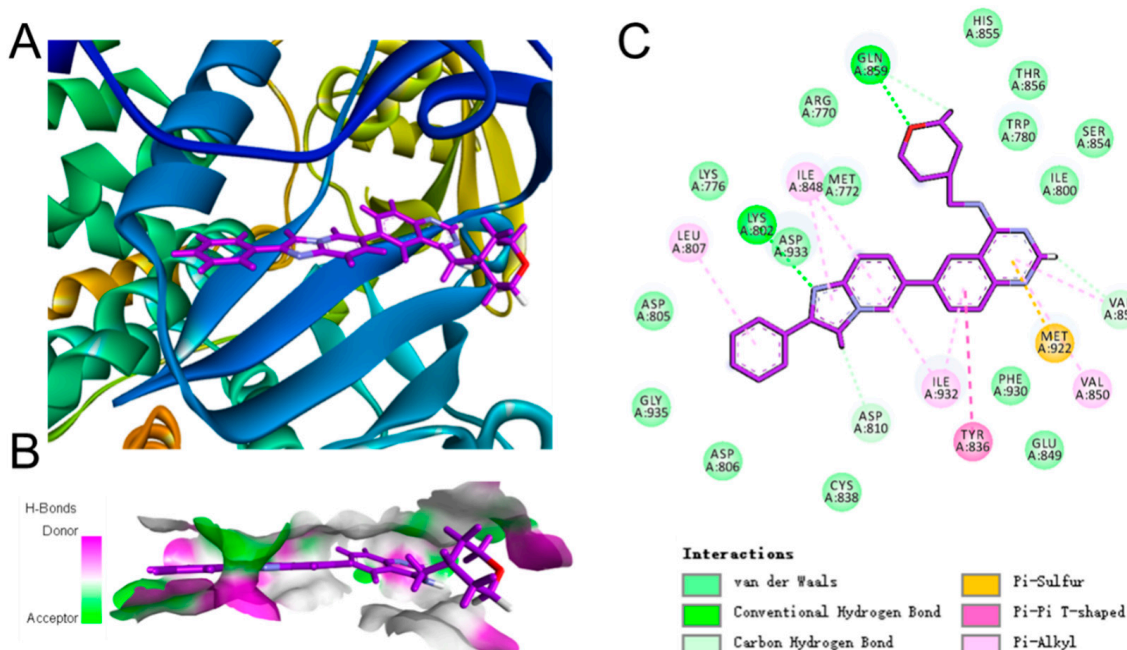


Figure 5. Molecular docking model of compound **13k** with PI3K α . (A) Docking of **13k** to the active site of PI3K α (PDB code: 4ZOP); (B) **13k** docked in the ATP-binding pocket of PI3K α ; (C) 2D binding model of **13k** and PI3K α . The image was observed with BIOVIA Discovery Studio Visualizer 4.5.

2.2.4. Compound **13k** Induced G2/M Phase Block in HCC827 Cells

It has shown that the anti-proliferative activity of PI3K α inhibitors was associated with cell cycle arrest [42]. Therefore, we examined the effects of **13k** on cell cycle distribution. As shown in Figure 6, **13k** treatment for 48 h resulted in a significant G2/M phase block of HCC827 cells (52.21%), when compared to the control group (20.84%). In order to elucidate the potential regulatory mechanism of **13k** on cell cycle, proteins associated with cell cycle regulation were detected using Western blot. As described in Figure 6C–G, the protein levels of cyclin B1, c-Myc and CDK1 were dose-dependently decreased by **13k** treatment. Additionally, both the total and phosphorylated proteins of CHK1 and CDC25A were also reduced by compound **13k**.

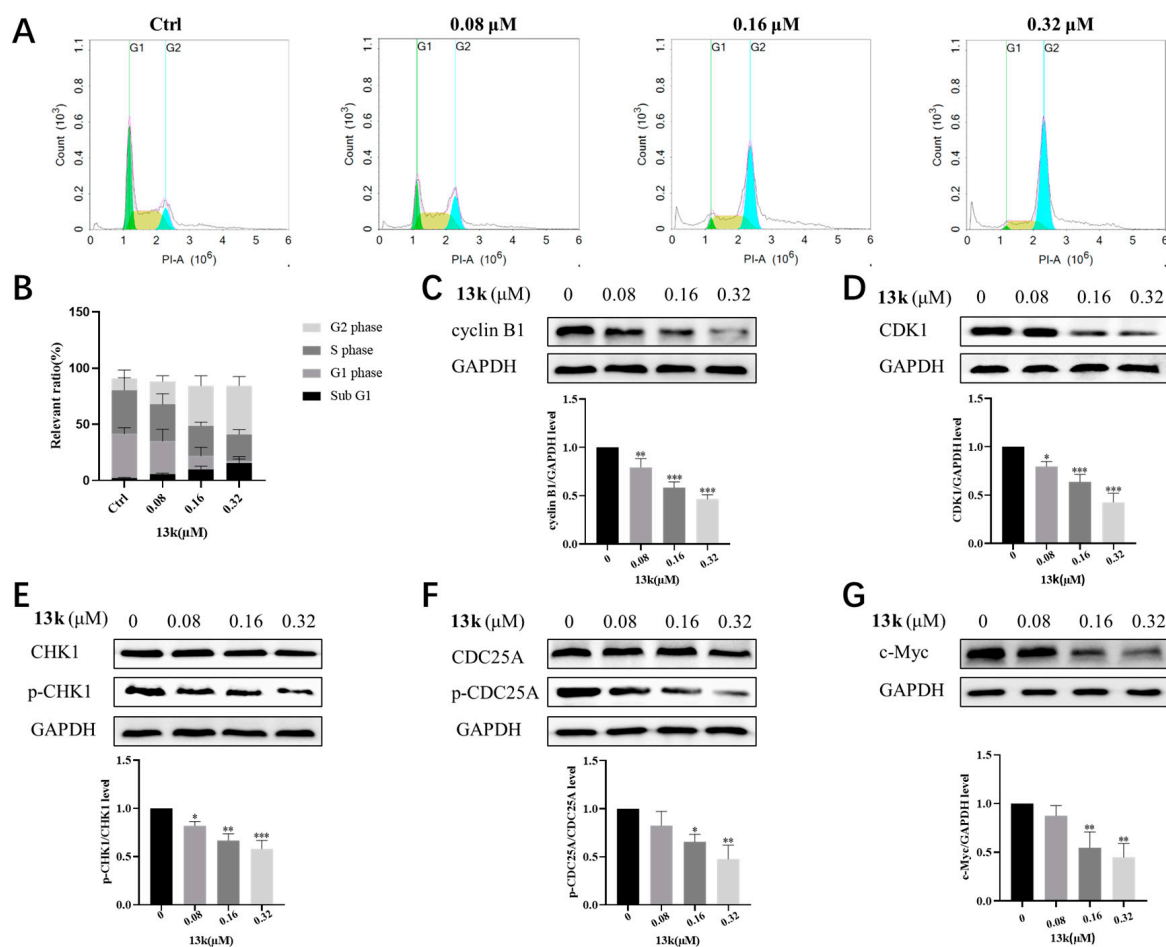


Figure 6. Effect of **13k** on the cell cycle of HCC827. (A) Compound **13k** alters the distribution of the cell cycle. Cells were treated with compound **13k** for 48 h, stained with propidium iodide mixed with RNase, incubated for 30 min at room temperature and protected from light and analysed by flow cytometry. ‘Ctrl’ refers to the control without the addition of compound **13k**. (B) Quantitative histograms of the different phases of the cell cycle. (C–G) Western blot analysis of protein expression associated with G2/M phase. Changes in the corresponding proteins were quantified using Image j. Each bar represents the mean \pm SD ($n = 3$) and was considered statistically significant when compared to the corresponding control values at * $p < 0.05$, ** $p < 0.01$ and *** $p < 0.001$.

2.2.5. Compound 13k Induced Cell Apoptosis

To further investigate the effects of **13k** on apoptosis, cells were treated with various doses of **13k** ranging from 0 to 0.32 μM . The percentage of apoptotic HCC827 cells was detected using Annexin V-FITC /PI double staining. The results showed that **13k** dose-dependently induced cellular apoptosis from 1.73–37.61%. In addition, Hoechst 33342 staining analysis indicated **13k** treatment caused cell shrinkage and DNA fragmentation, which resulted in an enhanced absorption and intensity of Hoechst staining. To further elucidate the mechanism of **13k**-induced apoptosis, the apoptosis-related protein levels was examined by Western blot. We found that compound **13k** increased the protein levels of cleaved caspase-9 and cleaved PARP in a concentration-dependent manner, while the ratios of Bax/Bcl-2 were upregulated, further indicating that compound **13k** promotes cell apoptosis (Figure 7).

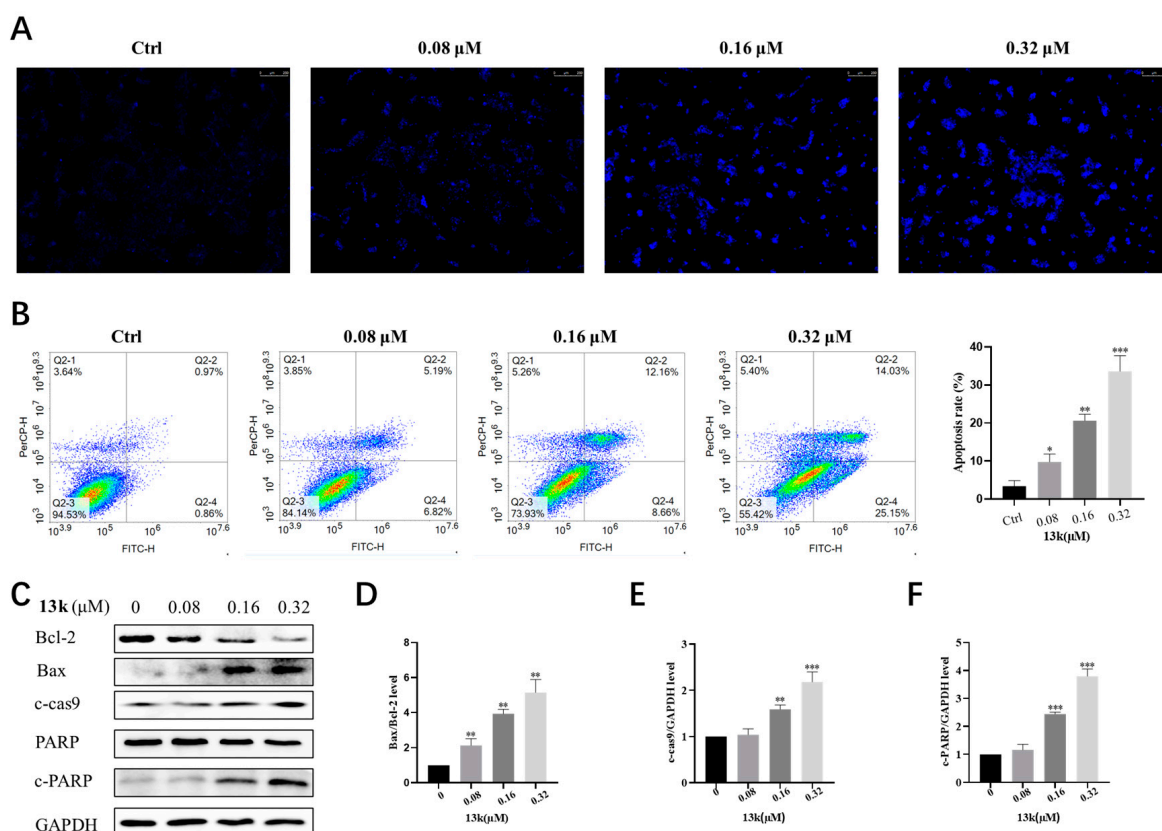


Figure 7. Compound **13k** induces apoptosis in HCC827 cells. (A) Apoptosis as well as nuclear morphology was measured by Hoechst 33342 staining after treatment of cells with compound **13k**, scale bar = 250 μM. (B) Apoptosis was quantified by flow cytometry using Annexin V-FITC/PI double staining. ‘Ctrl’ refers to the control without the addition of compound **13k**. (C–F) Western blot analysis was used to measure the regulation of apoptosis-associated proteins, using Image J for analysis. Each data is expressed as the mean ± SD of three parallel experiments (* $p < 0.05$, ** $p < 0.01$, *** $p < 0.001$ vs. control).

2.2.6. In 3D Spheroid Cell Inhibition Assay

The 3D cell culture has been proved to more realistically reproduce the interactions between cell–cell and cell–extracellular matrix interactions and more accurately simulate the actual microenvironment of cells in tissues [43–45]. These allow the cell behaviour characteristics of cells in 3D cell culture to be closer to the survival state in living organisms. Hence, it was widely applied in research fields including new drug screening, tumour cell system biology, stem cell research and functional tissue implantation [46–48]. Additionally, previous findings indicated that the phenotype of the 3D lung cancer tumour sphere in vitro is closer to that of real cancer tissue in vivo [49,50]. Thus, it is considered a reasonable method to evaluate the in vivo efficacy of active compounds in the early stages of new drug development [51]. To gain insight into the effects of long-term **13k** treatment, we used a 3D spheroid tumour growth model that was built using HCC827 cancer cells. After the 3D tumour spheres had been formed, they were treated with different concentrations of **13k** for 12 days, changing the drug-containing culture medium every 3 days. As shown in Figure 8, the tumour spheres were slightly contracted and flattened after treatment with 0.4 μM **13k** for 12 days. However, the spheres were gradually split and became loose and eventually collapsed when treated with increased concentration of **13k** (0.8 μM and 1.6 μM), indicating that **13k** could effectively inhibit the tumour sphere formation and has potential for further preclinical studies.

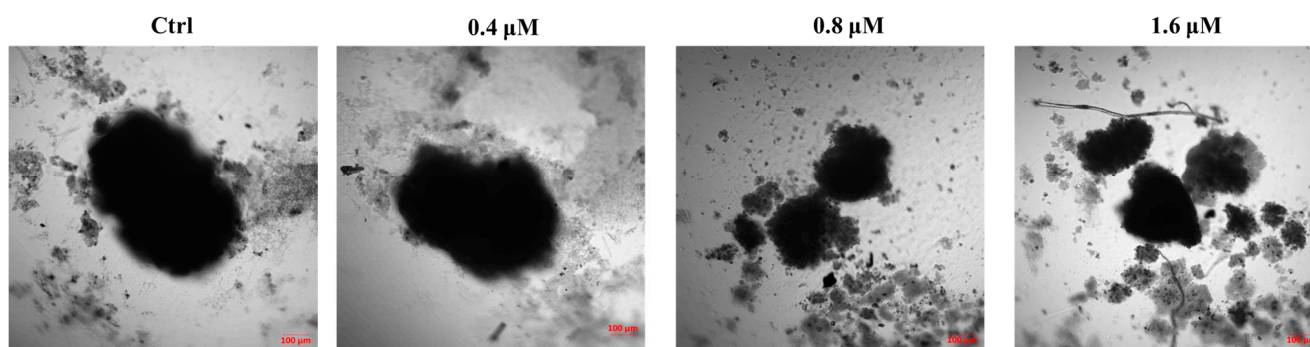


Figure 8. Effect of **13k** on HCC827 spheroid formation. HCC827 cells were seeded in ultralow attachment 96-well U bottom plates (40,000 cells/well) to generate tumour spheroids and treated with 5 fold of IC_{50} concentrations of **13k** for the spheroid assay. After initiation, the spheroids were treated with **13k** at the indicated concentrations every 3 days. After 12 days, pictures were taken with a ZEISS LSM 900 Airyscan 2 confocal laser scanning microscopy. ‘Ctrl’ refers to the control without the addition of compound **13k**.

3. Conclusions

In summary, a series of new 6-(imidazo[1,2-a]pyridin-6-yl)quinazoline derivatives (**10a–u** and **13a–k**) were designed, synthesized and evaluated for their *in vitro* anti-proliferative activities against five cancer cell lines (HCC827, A549, SH-SY5Y, HEL and MCF-7). As a result, most of the synthetic compounds showed submicromolar inhibitory activity against various tumour cell lines. Among them, **13k** is the most potent compound with IC_{50} values ranging from 0.09 μ M to 0.43 μ M against all the test cell lines. Moreover, compound **13k** showed strong inhibitory activity against PI3K α , and **13k** induced cell cycle arrest at G2/M phase and cell apoptosis of HCC827 cells by inhibition of PI3K α with an IC_{50} value of 1.94 nM. Compound **13k** showed better antitumour activity and PI3K α kinase activity compared to the lead compound **6b**. Therefore, compound **13k** could be a promising PI3K α inhibitor for the development of novel targeted antitumour drugs.

4. Experimental Procedure

4.1. Chemistry

4.1.1. Instruments and Materials

All reagents and solvents were commercially available and used without further purification. 1H NMR, ^{13}C NMR and ^{19}F NMR spectra were recorded with a 600, 150 and 565 MHz NMR spectrometer (Bruker AVANCE NEO), respectively. The NMR spectra were generated by using Mestrenova 12.0 as processing software, deuterated chloroform ($CDCl_3$) and dimethyl sulfoxide- d_6 ($DMSO-d_6$) as solvents, and tetramethylsilane (TMS) as an internal standard. All chemical shifts are expressed in ppm (δ), and the coupling constants (J) are expressed in hertz (Hz). The melting points of the compounds were determined using a Beijing micro melting point apparatus. High-resolution accurate mass measurements were performed on a quadrupole time-of-flight (QTOF) mass spectrometer (micro TOF-Q, Bruker Inc., Billerica, MA, USA) using electrospray ionisation (positive mode).

4.1.2. General Experimental Protocol for Preparation of Compounds **10a–u**

Preparation of 4-Chloro-6-iodoquinazoline (**2**)

A mixture of 6-iodoquinazolin-4(3H)-one (2.45 g, 9 mmol), N, N-diisopropylethylamine (2.33 g, 18 mmol), phosphorus oxychloride (2.76 g, 18 mmol) and anhydrous toluene (50 mL) was reacted at 80 $^{\circ}C$ for 4 h under argon atmosphere. After completion of the reaction (monitored by TLC), the crude reaction mixture was cooled, and the solvent was removed under reduced pressure. The mixture was extracted 2–3 times with ethyl acetate and saturated sodium bicarbonate solution. The organic phase was dried with anhydrous Na_2SO_4 and rotary dried under vacuum. The residue was purified through a column chromatography

on silica with EtOAc/PE to afford 4-chloro-6-iodoquinazoline 2 as white flocculent (2.27 g, 7.81 mmol, 86.83% yield), ESI-MS: m/z 291.5 $[M + H]^+$.

Steps for the Preparation of 6-Iodo-N-(4-methoxybenzyl)quinazolin-4-amine (5a)

A mixture of 4-chloro-6-iodoquinazoline (0.58 g, 2 mmol) and 4-Methoxybenzylamine (0.33 g, 2.4 mmol) was added to isopropanol (10 mL) and refluxed at 60 °C for 2 h under argon protection. After completion of the reaction (monitored by TLC), the solvent of the reaction mixture was removed under reduced pressure and extracted 2–3 times with ethyl acetate and saturated Na₂CO₃ solution. The organic phase was dried over anhydrous Na₂SO₄ and rotary dried under vacuum to form 6-iodo-N-(4-methoxybenzyl)quinazolin-4-amine 5a as white solid (0.60 g, 1.54 mmol, 77.0% yield), ESI-MS: m/z 392.1 $[M + H]^+$.

Compounds 5b–q were synthesized according to the procedure described in 5a. The ESI-MS information of compounds 5b–q is listed as below:

N-(cyclopropylmethyl)-6-iodoquinazolin-4-amine (5b)

Off-white solid, 91.2% yield, ESI-MS: m/z 326.0 $[M + H]^+$.

N-(4-fluorobenzyl)-6-iodoquinazolin-4-amine (5c)

Off-white solid, 77.8% yield, ESI-MS: m/z 380.0 $[M + H]^+$.

6-iodo-N-(4-(trifluoromethyl)benzyl)quinazolin-4-amine (5d)

Off-white solid, 86.1% yield, ESI-MS: m/z 430.2 $[M + H]^+$.

6-iodo-N-(3-methylbenzyl)quinazolin-4-amine (5e)

Pale yellow solid, 94.5% yield, ESI-MS: m/z 376.2 $[M + H]^+$.

N¹,N¹-diethyl-N²-(6-iodoquinazolin-4-yl)ethane-1,2-diamine (5f)

Pale yellow oily substance, 91.0% yield, ESI-MS: m/z 371.0 $[M + H]^+$.

6-iodo-N-(2-methylbenzyl)quinazolin-4-amine (5g)

Pale yellow solid, 95.3% yield, ESI-MS: m/z 376.0 $[M + H]^+$.

6-iodo-N-(pyridin-2-ylmethyl)quinazolin-4-amine (5h)

Pale yellow solid, 92.1% yield, ESI-MS: m/z 385.2 $[M + Na]^+$.

N-(2-fluorobenzyl)-6-iodoquinazolin-4-amine (5i)

Off-white solid, 61.9% yield, ESI-MS: m/z 380.0 $[M + H]^+$.

N-(3-fluorophenyl)-6-iodoquinazolin-4-amine (5j)

Pale yellow solid, 85.3% yield, ESI-MS: m/z 366.1 $[M + H]^+$.

N-(3,5-dimethoxyphenyl)-6-iodoquinazolin-4-amine (5k)

Pale yellow solid, 90.7% yield, ESI-MS: m/z 408.2 $[M + H]^+$.

6-iodo-N-(pyridin-3-ylmethyl)quinazolin-4-amine (5l)

Pink solid, 94.2% yield, ESI-MS: m/z 385.2 $[M + H]^+$.

N-(2,3-difluorophenyl)-6-iodoquinazolin-4-amine (5m)

Off-white solid, 93.6% yield, ESI-MS: m/z 384.1 $[M + H]^+$.

6-iodo-N-methyl-N-(p-tolyl)quinazolin-4-amine (5n)

Pale yellow solid, 94.0% yield, ESI-MS: m/z 376.0 $[M + H]^+$.

N-ethyl-6-iodo-N-phenylquinazolin-4-amine (5o)

Pale yellow solid, 95.7% yield, ESI-MS: m/z 376.0 [M + H]⁺.

6-iodo-N-(1H-pyrazol-3-yl)quinazolin-4-amine (5p)

White solid, 91.5% yield, ESI-MS: m/z 338.1 [M + H]⁺.

6-iodo-N-((tetrahydro-2H-pyran-4-yl)methyl)quinazolin-4-amine (5q)

White solid, 90.1% yield, ESI-MS: m/z 392.0 [M + Na]⁺.

Procedure for the Preparation of 6-(6-Aminopyridin-3-yl)-N-(4-methoxybenzyl)quinazolin-4-amine (7a)

The 6-iodo-N-(4-methoxybenzyl)quinazolin-4-amine **5a** (0.6 g, 1.5 mmol), 5-(4,4,5,5-tetramethyl-1,3,2-dioxaborolan-2-yl)pyridin-2-amine (0.34 g, 1.5 mmol) and K₂CO₃ (0.64 g, 4.6 mmol) were added to 15 mL of solvent [$V_{(1,4\text{-dioxane})}:V_{(\text{water})} = 4:1$]. The mixture was heated to 100 °C under a protective atmosphere of argon followed by the addition of Pd(dppf)Cl₂. The mixture continues to be stirred under these conditions for a further 4–6 h. After completion of the reaction (monitored by TLC), 1,4-dioxane and water were removed under reduced pressure, and the residue was purified through a column chromatography on silica with dichloromethane/methanol to afford white solid 6-(6-aminopyridin-3-yl)-N-(4-methoxybenzyl)quinazolin-4-amine **7a** (0.36 g, 0.99 mmol, 66.6% yield), ESI-MS: m/z 358.1 [M + H]⁺.

Compounds **7b–o** were synthesized according to the procedure described in **7a**. The ESI-MS information of compounds **7b–o** is listed as below:

6-(6-Aminopyridin-3-yl)-N-(cyclopropylmethyl)quinazolin-4-amine (7b)

Off-white solid, 71.2% yield, ESI-MS: m/z 291.1 [M + H]⁺.

6-(6-Aminopyridin-3-yl)-N-(4-fluorobenzyl)quinazolin-4-amine (7c)

Off-white solid, 92.2% yield, ESI-MS: m/z 246.1 [M + H]⁺.

6-(6-Aminopyridin-3-yl)-N-(4-(trifluoromethyl)benzyl)quinazolin-4-amine (7d)

Off-white solid, 85.7% yield, ESI-MS: m/z 396.1 [M + H]⁺.

6-(6-Aminopyridin-3-yl)-N-(3-methylbenzyl)quinazolin-4-amine (7e)

Off-white solid, 73.4% yield, ESI-MS: m/z 342.1 [M + H]⁺.

N1-(6-(6-aminopyridin-3-yl)quinazolin-4-yl)-N2,N2-diethylethane-1,2-diamine (7f)

Brown solid, 82.9% yield, ESI-MS: m/z 359.1 [M + Na]⁺.

6-(6-Aminopyridin-3-yl)-N-(2-methylbenzyl)quinazolin-4-amine (7g)

Off-white solid, 76.3% yield, ESI-MS: m/z 342.1 [M + H]⁺.

6-(6-Aminopyridin-3-yl)-N-(pyridin-2-ylmethyl)quinazolin-4-amine (7h)

Yellow solid, 70.6% yield, ESI-MS: m/z 328.1 [M + H]⁺.

6-(6-Aminopyridin-3-yl)-N-(2-fluorobenzyl)quinazolin-4-amine (7i)

Off-white solid, 86.3% yield, ESI-MS: m/z 346.1 [M + H]⁺.

6-(6-Aminopyridin-3-yl)-N-(3-fluorophenyl)quinazolin-4-amine (7j)

Pale yellow solid, 77.6% yield, ESI-MS: m/z 332.1 [M + H]⁺.

6-(6-Aminopyridin-3-yl)-N-(3,5-dimethoxyphenyl)quinazolin-4-amine (7k)

Yellow solid, 81.3% yield, ESI-MS: m/z 396.1 [M + Na]⁺.

6-(6-Aminopyridin-3-yl)-N-(pyridin-3-ylmethyl)quinazolin-4-amine (**7l**)

Off-white solid, 67.6% yield, ESI-MS: m/z 329.1 [M + H]⁺.

6-(6-Aminopyridin-3-yl)-N-(2,3-difluorophenyl)quinazolin-4-amine (**7m**)

White solid, 88.7% yield, ESI-MS: m/z 352.1 [M + Na]⁺.

6-(6-Aminopyridin-3-yl)-N-methyl-N-(p-tolyl)quinazolin-4-amine (**7n**)

Pale yellow solid, 79.8% yield, ESI-MS: m/z 342.1 [M + H]⁺.

6-(6-Aminopyridin-3-yl)-N-ethyl-N-phenylquinazolin-4-amine (**7o**)

Yellow solid, 75.7% yield, ESI-MS: m/z 342.1 [M + H]⁺.

Procedure for the Preparation of Ethyl 6-(4-((4-Methoxybenzyl)amino)quinazolin-6-yl)imidazo[1,2-a]pyridine-2-carboxylate (**10a**) or Methyl 6-(4-((4-methoxybenzyl)amino)quinazolin-6-yl)imidazo[1,2-a]pyridine-2-carboxylate (**10o**)

A mixture of 6-(6-aminopyridin-3-yl)-N-(4-methoxybenzyl)quinazolin-4-amine **7a** (0.18 g, 0.5 mmol), ethyl bromopyruvate (0.29 g, 1.5 mmol) or methyl bromopyruvate (0.27 g, 1.5 mmol) and NaHCO₃ (0.13 g, 1.5 mmol) was added to EtOH (5 mL), and the mixture was warmed to 80 °C and refluxed by condensation under argon for 4 h. After completion of the reaction (monitored by TLC), the solvents were removed under reduced pressure and the residue was purified through a column chromatography on silica with dichloromethane/methanol to obtain ethyl 6-(4-((4-methoxybenzyl)amino)quinazolin-6-yl)imidazo[1,2-a]pyridine-2-carboxylate **10a** or methyl 6-(4-((4-methoxybenzyl)amino)quinazolin-6-yl)imidazo[1,2-a]pyridine-2-carboxylate **10o**; **10a** as white solid (0.142 g, 0.31 mmol, 62.0% yield), m.p. 131.2–133.6 °C. ¹H NMR (600 MHz, Chloroform-*d*) δ 8.69 (s, 1H), 8.22 (s, 1H), 8.09 (s, 1H), 8.05 (s, 1H), 7.89 (d, *J* = 8.6 Hz, 1H), 7.83 (d, *J* = 8.5 Hz, 1H), 7.53 (d, *J* = 9.0 Hz, 1H), 7.40 (d, *J* = 9.4 Hz, 1H), 7.33 (d, *J* = 8.1 Hz, 2H), 7.24–7.17 (m, 1H), 6.83 (d, *J* = 8.0 Hz, 2H), 4.84 (s, 2H), 4.37 (q, *J* = 7.1 Hz, 2H), 3.76 (s, 3H), 1.37 (t, *J* = 7.1 Hz, 3H). ¹³C NMR (150 MHz, CDCl₃) δ 163.1, 159.5, 159.2, 156.0, 149.1, 144.3, 137.3, 134.1, 131.2, 130.2, 129.6 (2C), 129.2, 127.5, 126.9, 123.6, 120.0, 118.7, 117.3, 115.4, 114.1 (2C), 61.3, 55.3, 44.9, 14.4. HRMS (ESI): calcd for C₂₆H₂₄O₃N₅ [M + H]⁺ m/z 454.1874, found 454.1866; C₂₆H₂₃O₃N₅Na [M + Na]⁺ m/z 476.1693, found 476.1687; **10o** as white solid (0.096 g, 0.218 mmol, 43.7% yield), m.p. 138.6–140.9 °C. ¹H NMR (600 MHz, DMSO-*d*₆) δ 9.25 (s, 1H), 9.04 (d, *J* = 0.8 Hz, 1H), 8.73 (s, 1H), 8.54 (s, 2H), 8.13 (d, *J* = 8.7 Hz, 1H), 7.86 (d, *J* = 9.6 Hz, 1H), 7.80 (d, *J* = 8.6 Hz, 1H), 7.75 (d, *J* = 9.7 Hz, 1H), 7.34 (d, *J* = 8.7 Hz, 2H), 6.89 (d, *J* = 8.7 Hz, 2H), 4.77 (d, *J* = 5.7 Hz, 2H), 3.85 (s, 3H), 3.71 (s, 3H). ¹³C NMR (150 MHz, DMSO) δ 163.0, 159.5, 158.4, 154.9, 148.5, 143.9, 135.9, 133.6, 131.2, 130.9, 130.9, 128.9 (2C), 126.8, 125.5, 125.1, 120.8, 118.5, 118.0, 115.0, 113.8 (2C), 55.1, 51.7, 43.4. HRMS (ESI): calcd for C₂₅H₂₂O₃N₅ [M + H]⁺ m/z 440.1717, found 440.1711.

Compounds **10b–n** and **10p–u** were synthesized according to the procedure described in **10a** or **10o**. The information of compounds **10b–n** and **10p–u** is listed as below:

Ethyl 6-(4-((Cyclopropylmethyl)amino)quinazolin-6-yl)imidazo[1,2-a]pyridine-2-carboxylate (**10b**)

White solid, 49.8% yield, m.p. 128.5–130.8 °C. ¹H NMR (600 MHz, DMSO-*d*₆) δ 9.03 (s, 1H), 8.64 (d, *J* = 2.1 Hz, 1H), 8.57 (d, *J* = 4.9 Hz, 2H), 8.47 (s, 1H), 8.09 (dd, *J* = 8.7, 2.0 Hz, 1H), 7.87 (dd, *J* = 9.6, 1.9 Hz, 1H), 7.79 (dd, *J* = 9.1, 6.6 Hz, 2H), 4.33 (q, *J* = 7.1 Hz, 2H), 3.48–3.42 (m, 2H), 1.33 (t, *J* = 7.1 Hz, 3H), 1.22 (ddd, *J* = 11.6, 7.3, 5.3 Hz, 1H), 0.53–0.46 (m, 2H), 0.34–0.29 (m, 2H). ¹³C NMR (150 MHz, DMSO) δ 162.6, 159.5, 155.5, 148.9, 143.8, 136.2, 133.2, 130.7, 128.4, 126.9, 125.8, 125.0, 120.7, 118.4, 118.0, 115.2, 60.3, 45.1, 14.3, 10.6, 3.6 (2C). HRMS (ESI): calcd for C₂₂H₂₂O₂N₅ [M + H]⁺ m/z 388.1768, found 388.1760; C₂₂H₂₁O₂N₅Na [M + Na]⁺ m/z 410.1588, found 410.1580.

Ethyl 6-(4-((4-Fluorobenzyl)amino)quinazolin-6-yl)imidazo[1,2-a]pyridine-2-carboxylate (10c)

White solid, 55.1% yield, m.p. 127.8–129.1 °C. ¹H NMR (600 MHz, DMSO-*d*₆) δ 9.04 (t, *J* = 1.3 Hz, 1H), 9.01 (t, *J* = 5.9 Hz, 1H), 8.68 (d, *J* = 2.2 Hz, 1H), 8.56 (s, 1H), 8.49 (s, 1H), 8.12 (dd, *J* = 8.7, 2.0 Hz, 1H), 7.87 (dd, *J* = 9.6, 1.9 Hz, 1H), 7.82 (d, *J* = 8.7 Hz, 1H), 7.79 (d, *J* = 9.5 Hz, 1H), 7.45 (dd, *J* = 8.5, 5.7 Hz, 2H), 7.16 (t, *J* = 8.9 Hz, 2H), 4.81 (d, *J* = 5.7 Hz, 2H), 4.33 (q, *J* = 7.1 Hz, 2H), 1.33 (t, *J* = 7.1 Hz, 3H). ¹³C NMR (150 MHz, DMSO) δ 162.6, 162.1, 160.5, 159.4, 155.4, 148.9, 143.9, 136.2, 135.5, 133.4, 130.9, 129.4, 129.4, 128.5, 126.8, 125.7, 125.0, 120.7, 118.4, 118.0, 115.2, 115.0, 60.3, 43.0, 14.3. ¹⁹F NMR (565 MHz, DMSO) δ −115.99. HRMS (ESI): calcd for C₂₅H₂₁O₂N₅F [M + H]⁺ *m/z* 442.1674, found 442.1667; C₂₅H₂₀O₂N₅FNa [M + Na]⁺ *m/z* 464.1493, found 464.1489.

Ethyl 6-(4-((4-(Trifluoromethyl)benzyl)amino)quinazolin-6-yl)imidazo[1,2-a]pyridine-2-carboxylate (10d)

White solid, 56.8% yield, m.p. 129.8–131.1 °C. ¹H NMR (600 MHz, DMSO-*d*₆) δ 9.14 (t, *J* = 6.0 Hz, 1H), 9.05 (s, 1H), 8.70 (s, 1H), 8.56 (s, 1H), 8.49 (s, 1H), 8.14 (d, *J* = 8.5 Hz, 1H), 7.87 (d, *J* = 9.4 Hz, 1H), 7.84 (d, *J* = 8.6 Hz, 1H), 7.80 (d, *J* = 9.4 Hz, 1H), 7.70 (d, *J* = 8.0 Hz, 2H), 7.61 (d, *J* = 8.1 Hz, 2H), 4.92 (d, *J* = 5.6 Hz, 2H), 4.33 (q, *J* = 7.1 Hz, 2H), 1.33 (t, *J* = 7.1 Hz, 3H). ¹³C NMR (150 MHz, DMSO) δ 162.6, 159.5, 155.3, 148.7, 144.3, 143.8, 136.2, 133.5, 131.0, 128.4, 128.0 (2C), 127.7, 126.7, 125.6, 125.3 (2C), 125.0, 123.5, 120.7, 118.4, 118.0, 115.1, 60.3, 43.4, 14.3. ¹⁹F NMR (565 MHz, DMSO) δ −60.78. HRMS (ESI): calcd for C₂₆H₂₁O₂N₅F₃ [M + H]⁺ *m/z* 492.1642, found 492.1632; C₂₆H₂₀O₂N₅F₃Na [M + Na]⁺ *m/z* 514.1461, found 514.1452.

Ethyl 6-(4-((3-Methylbenzyl)amino)quinazolin-6-yl)imidazo[1,2-a]pyridine-2-carboxylate (10e)

Off-white solid 53.0% yield, m.p. 130.1–132.5 °C. ¹H NMR (600 MHz, DMSO-*d*₆) δ 9.03 (s, 1H), 9.01 (t, *J* = 5.9 Hz, 1H), 8.70 (s, 1H), 8.55 (s, 1H), 8.50 (s, 1H), 8.12 (d, *J* = 7.9 Hz, 1H), 7.87 (d, *J* = 9.4 Hz, 1H), 7.82 (d, *J* = 8.6 Hz, 1H), 7.79 (d, *J* = 9.5 Hz, 1H), 7.20 (dd, *J* = 12.5, 7.3 Hz, 3H), 7.06 (d, *J* = 7.1 Hz, 1H), 4.80 (d, *J* = 5.7 Hz, 2H), 4.33 (q, *J* = 7.1 Hz, 2H), 2.28 (s, 3H), 1.33 (t, *J* = 7.1 Hz, 3H). ¹³C NMR (150 MHz, DMSO) δ 162.6, 159.5, 155.4, 148.7, 143.9, 139.2, 137.5, 136.2, 133.4, 130.9, 128.3, 128.3, 128.0, 127.6, 126.8, 125.7, 125.0, 124.5, 120.7, 118.5, 118.0, 115.2, 60.4, 43.7, 21.1, 14.3. HRMS (ESI): calcd for C₂₆H₂₄O₂N₅ [M + H]⁺ *m/z* 438.1925, found 438.1918; C₂₆H₂₃O₂N₅Na [M + Na]⁺ *m/z* 460.1744, found 460.1737.

Ethyl 6-(4-((2-(Diethylamino)ethyl)amino)quinazolin-6-yl)imidazo[1,2-a]pyridine-2-carboxylate (10f)

Brown solid, 42.1% yield, m.p. 235.7–237.9 °C. ¹H NMR (600 MHz, DMSO-*d*₆) δ 9.28 (s, 1H), 9.24 (s, 1H), 8.98 (s, 1H), 8.51 (d, *J* = 11.6 Hz, 2H), 8.16 (d, *J* = 8.7 Hz, 1H), 8.06 (d, *J* = 9.6 Hz, 1H), 7.81 (d, *J* = 8.6 Hz, 1H), 7.74 (d, *J* = 9.4 Hz, 1H), 4.33 (q, *J* = 7.1 Hz, 2H), 3.94 (s, 2H), 3.17 (s, 6H), 1.33 (t, *J* = 7.1 Hz, 3H), 1.22 (s, 6H). ¹³C NMR (150 MHz, DMSO) δ 162.6, 159.6, 155.2, 148.8, 143.9, 136.1, 133.1, 130.6, 128.3, 126.7, 125.3, 125.2, 121.1, 118.3, 117.9, 115.4, 60.4 (2C), 46.6 (3C), 14.3 (3C). HRMS (ESI): calcd for C₂₄H₂₉O₂N₆ [M + H]⁺ *m/z* 433.2347, found 433.2341.

Ethyl 6-(4-((2-Methylbenzyl)amino)quinazolin-6-yl)imidazo[1,2-a]pyridine-2-carboxylate (10g)

Pink solid, 45.8% yield, m.p. 149.6–151.7 °C. ¹H NMR (600 MHz, DMSO-*d*₆) δ 9.05 (s, 1H), 8.94 (s, 1H), 8.76 (s, 1H), 8.56 (s, 1H), 8.51 (s, 1H), 8.15 (d, *J* = 8.6 Hz, 1H), 7.88 (d, *J* = 9.4 Hz, 1H), 7.84 (d, *J* = 8.5 Hz, 1H), 7.80 (d, *J* = 9.5 Hz, 1H), 7.30 (d, *J* = 7.3 Hz, 1H), 7.22–7.14 (m, 3H), 4.81 (d, *J* = 5.4 Hz, 2H), 4.33 (q, *J* = 7.1 Hz, 2H), 2.37 (s, 3H), 1.33 (t, *J* = 7.0 Hz, 3H). ¹³C NMR (150 MHz, DMSO) δ 162.6, 159.5, 155.2, 143.8, 136.5, 136.2, 135.9, 133.5, 133.5, 131.0, 130.0, 128.0, 127.4, 127.0, 126.8, 125.8, 125.7, 125.0, 120.8, 118.4, 118.0, 115.1, 60.3, 42.1, 18.8, 14.3. HRMS (ESI): calcd for C₂₆H₂₄O₂N₅ [M + H]⁺ *m/z* 438.1925, found 438.1917; C₂₆H₂₃O₂N₅Na [M + Na]⁺ *m/z* 460.1744, found 460.1735.

Ethyl 6-(4-((Pyridin-2-ylmethyl)amino)quinazolin-6-yl)imidazo[1,2-a]pyridine-2-carboxylate (10h)

Yellow solid, 57.3% yield, m.p. 129.6–131.5 °C. ¹H NMR (600 MHz, DMSO-*d*₆) δ 9.20–9.14 (m, 1H), 9.05 (s, 1H), 8.73 (s, 1H), 8.58–8.51 (m, 2H), 8.47 (s, 1H), 8.14 (d, *J* = 8.6 Hz, 1H), 7.88 (d, *J* = 9.5 Hz, 1H), 7.84–7.78 (m, 2H), 7.73 (t, *J* = 7.6 Hz, 1H), 7.39 (d, *J* = 7.9 Hz, 1H), 7.29–7.24 (m, 1H), 4.92 (d, *J* = 5.7 Hz, 2H), 4.32 (q, *J* = 7.1 Hz, 2H), 1.33 (t, *J* = 7.1 Hz, 3H). ¹³C NMR (150 MHz, DMSO) δ 162.6, 159.6, 158.5, 155.3, 149.0, 148.6, 143.8, 136.8, 136.2, 133.4, 130.9, 128.3, 126.7, 125.6, 125.0, 122.2, 121.2, 120.7, 118.4, 118.0, 115.2, 60.3, 45.7, 14.3. HRMS (ESI): calcd for C₂₄H₂₁O₂N₆ [M + H]⁺ *m/z* 425.1721, found 425.1712; C₂₄H₂₀O₂N₆Na [M + Na]⁺ *m/z* 447.1540, found 447.1532.

Ethyl 6-(4-((2-Fluorobenzyl)amino)quinazolin-6-yl)imidazo[1,2-a]pyridine-2-carboxylate (10i)

Off-white solid, 59.2% yield, m.p. 142.3–144.6 °C. ¹H NMR (600 MHz, DMSO-*d*₆) δ 9.48 (s, 1H), 9.08 (s, 1H), 8.81 (s, 1H), 8.60 (s, 1H), 8.55 (s, 1H), 8.19 (d, *J* = 8.4 Hz, 1H), 7.88 (d, *J* = 9.4 Hz, 1H), 7.85 (d, *J* = 8.4 Hz, 1H), 7.78 (d, *J* = 9.4 Hz, 1H), 7.46 (t, *J* = 7.6 Hz, 1H), 7.33 (q, *J* = 6.9 Hz, 1H), 7.22 (t, *J* = 9.3 Hz, 1H), 7.16 (t, *J* = 7.4 Hz, 1H), 4.90 (d, *J* = 5.2 Hz, 2H), 4.33 (q, *J* = 7.0 Hz, 2H), 1.33 (t, *J* = 7.0 Hz, 3H). ¹³C NMR (150 MHz, DMSO) δ 162.5, 161.1, 159.8, 159.5, 154.3, 143.8, 136.2, 134.1, 131.6, 129.6, 129.1, 126.7, 126.5, 125.3, 125.2, 124.4, 121.0, 118.4, 118.0, 115.3, 115.2, 114.7, 60.3, 38.0, 14.3. ¹⁹F NMR (565 MHz, DMSO) δ −118.51. HRMS (ESI): calcd for C₂₅H₂₁O₂N₅F [M + H]⁺ *m/z* 442.1674, found 442.1664; C₂₅H₂₀O₂N₅FNa [M + Na]⁺ *m/z* 464.1493, found 464.1486.

Ethyl 6-(4-((3-Fluorophenyl)amino)quinazolin-6-yl)imidazo[1,2-a]pyridine-2-carboxylate (10j)

Yellow solid, 46.7% yield, m.p. 148.3–150.1 °C. ¹H NMR (600 MHz, DMSO-*d*₆) δ 10.09 (s, 1H), 9.08 (s, 1H), 8.86 (s, 1H), 8.68 (s, 1H), 8.56 (s, 1H), 8.19 (d, *J* = 8.7 Hz, 1H), 7.92 (t, *J* = 8.0 Hz, 3H), 7.82 (d, *J* = 9.4 Hz, 1H), 7.68 (d, *J* = 8.2 Hz, 1H), 7.45 (q, *J* = 7.8 Hz, 1H), 6.98 (td, *J* = 8.5, 2.6 Hz, 1H), 4.33 (q, *J* = 7.1 Hz, 2H), 1.33 (t, *J* = 7.1 Hz, 3H). ¹³C NMR (150 MHz, DMSO) δ 162.9, 162.6, 161.3, 157.7, 154.6, 149.2, 143.9, 136.3, 134.3, 131.6, 130.1, 128.7, 126.9, 125.6, 125.4, 120.8, 118.5, 118.1, 117.9, 115.4, 110.4, 109.1, 60.4, 14.3. ¹⁹F NMR (565 MHz, DMSO) δ −112.46. HRMS (ESI): calcd for C₂₄H₁₈O₂N₅FNa [M + Na]⁺ *m/z* 450.1337, found 450.1328.

Ethyl 6-(4-((3,5-dimethoxyphenyl)amino)quinazolin-6-yl)imidazo[1,2-a]pyridine-2-carboxylate (10k)

Yellow solid, 50.2% yield, m.p. 156.2–158.3 °C. ¹H NMR (600 MHz, DMSO-*d*₆) δ 9.90 (s, 1H), 9.09 (s, 1H), 8.87 (s, 1H), 8.66 (s, 1H), 8.57 (s, 1H), 8.19 (d, *J* = 8.4 Hz, 1H), 7.94 (d, *J* = 9.3 Hz, 1H), 7.90 (d, *J* = 8.6 Hz, 1H), 7.82 (d, *J* = 9.4 Hz, 1H), 7.19 (s, 2H), 6.34 (s, 1H), 4.33 (q, *J* = 7.1 Hz, 2H), 3.78 (s, 6H), 1.34 (t, *J* = 7.1 Hz, 3H). ¹³C NMR (150 MHz, DMSO) δ 162.6, 160.4 (2C), 157.8, 154.6, 148.9, 143.9, 140.6, 136.2, 134.2, 131.5, 128.4, 126.9, 125.6, 125.3, 120.8, 118.5, 118.0, 115.4, 100.8 (2C), 95.8, 60.3, 55.3 (2C), 14.3. HRMS (ESI): calcd for C₂₆H₂₄O₄N₅ [M + H]⁺ *m/z* 470.1823, found 470.1809; C₂₆H₂₃O₄N₅Na [M + Na]⁺ *m/z* 492.1642, found 492.1633.

Ethyl 6-(4-((2,3-difluorophenyl)amino)quinazolin-6-yl)imidazo[1,2-a]pyridine-2-carboxylate (10l)

White solid, 55.3% yield, m.p. 131.2–133.6 °C. ¹H NMR (600 MHz, DMSO-*d*₆) δ 10.21 (s, 1H), 9.10 (s, 1H), 8.83 (s, 1H), 8.57 (d, *J* = 7.1 Hz, 2H), 8.23 (d, *J* = 8.7 Hz, 1H), 8.02–7.86 (m, 2H), 7.82 (d, *J* = 9.5 Hz, 1H), 7.39 (s, 2H), 7.30 (s, 1H), 4.33 (q, *J* = 7.1 Hz, 2H), 1.33 (t, *J* = 7.1 Hz, 3H). ¹³C NMR (150 MHz, DMSO) δ 162.6, 158.4, 154.9, 151.3, 151.2, 149.6, 149.6, 143.9, 136.3, 134.2, 131.6, 128.6, 126.7, 125.5, 125.3, 124.3, 123.2, 121.0, 118.5, 118.1, 115.1, 114.5, 60.4, 14.3. ¹⁹F NMR (565 MHz, DMSO) δ −138.40, −142.37. HRMS (ESI): calcd for C₂₄H₁₈O₂N₅F₂ [M + H]⁺ *m/z* 446.1423, found 446.1411; C₂₄H₁₇O₂N₅F₂Na [M + Na]⁺ *m/z* 468.1243, found 468.1231.

Ethyl 6-(4-(Ethyl(phenyl)amino)quinazolin-6-yl)imidazo[1,2-a]pyridine-2-carboxylate (10m)

Pink flocculent, 63.1% yield, m.p. 176.7–177.8 °C. ¹H NMR (600 MHz, DMSO-*d*₆) δ 8.74 (s, 1H), 8.50 (s, 1H), 8.45 (s, 1H), 7.97 (dd, *J* = 8.7, 2.1 Hz, 1H), 7.85 (d, *J* = 8.6 Hz, 1H), 7.60–7.55 (m, 3H), 7.50 (t, *J* = 7.4 Hz, 1H), 7.38 (d, *J* = 7.6 Hz, 2H), 7.10 (d, *J* = 2.1 Hz,

1H), 6.86 (dd, $J = 9.5, 1.8$ Hz, 1H), 4.32 (q, $J = 7.1$ Hz, 2H), 4.20 (q, $J = 6.9$ Hz, 2H), 1.33 (t, $J = 7.1$ Hz, 3H), 1.25 (t, $J = 7.0$ Hz, 3H). ^{13}C NMR (150 MHz, DMSO) δ 162.5, 160.0, 154.5, 151.1, 145.8, 143.6, 136.2, 131.9, 130.5 (2C), 130.4, 129.1, 127.3, 127.2 (2C), 125.8, 125.4, 124.7, 124.0, 118.4, 117.9, 115.8, 60.4, 48.2, 14.3, 11.7. HRMS (ESI): calcd for $\text{C}_{26}\text{H}_{24}\text{O}_2\text{N}_5$ $[\text{M} + \text{H}]^+$ m/z 438.1925, found 438.1916; $\text{C}_{26}\text{H}_{23}\text{O}_2\text{N}_5\text{Na}$ $[\text{M} + \text{Na}]^+$ m/z 460.1744, found 460.1735.

Ethyl 6-(4-((Pyridin-3-ylmethyl)amino)quinazolin-6-yl)imidazo[1,2-a]pyridine-2-carboxylate (10n)

White solid, 47.3% yield, m.p. 120.3–122.4 °C. ^1H NMR (600 MHz, DMSO- d_6) δ 9.08 (t, $J = 5.9$ Hz, 1H), 9.04 (s, 1H), 8.66 (d, $J = 7.1$ Hz, 2H), 8.55 (s, 1H), 8.51 (s, 1H), 8.47 (d, $J = 4.8$ Hz, 1H), 8.13 (d, $J = 8.6$ Hz, 1H), 7.87 (d, $J = 9.5$ Hz, 1H), 7.84–7.77 (m, 3H), 7.36 (dd, $J = 7.9, 4.7$ Hz, 1H), 4.85 (d, $J = 5.7$ Hz, 2H), 4.33 (q, $J = 7.1$ Hz, 2H), 1.33 (t, $J = 7.1$ Hz, 3H). ^{13}C NMR (150 MHz, DMSO) δ 162.6, 159.5, 155.3, 149.0, 148.7, 148.2, 143.8, 136.2, 135.3, 134.8, 133.5, 131.0, 128.4, 126.8, 125.7, 125.0, 123.6, 120.7, 118.4, 118.0, 115.1, 60.4, 41.5, 14.3. HRMS (ESI): calcd for $\text{C}_{24}\text{H}_{21}\text{O}_2\text{N}_6$ $[\text{M} + \text{H}]^+$ m/z 425.1721, found 425.1711; $\text{C}_{24}\text{H}_{20}\text{O}_2\text{N}_6\text{Na}$ $[\text{M} + \text{Na}]^+$ m/z 447.1540, found 447.1534.

Methyl 6-(4-((2-Methylbenzyl)amino)quinazolin-6-yl)imidazo[1,2-a]pyridine-2-carboxylate (10p)

Off-white solid, 36.7% yield, m.p. 150.3–152.5 °C. ^1H NMR (600 MHz, DMSO- d_6) δ 9.05 (s, 2H), 8.77 (s, 1H), 8.57 (s, 1H), 8.53 (s, 1H), 8.23–8.08 (m, 1H), 7.96–7.70 (m, 3H), 7.30 (d, $J = 7.2$ Hz, 1H), 7.24–7.11 (m, 3H), 4.81 (d, $J = 4.7$ Hz, 2H), 3.86 (s, 3H), 2.37 (s, 3H). ^{13}C NMR (150 MHz, DMSO) δ 163.0, 159.6, 155.0, 147.7, 143.9, 136.4, 135.9, 133.7, 131.7, 131.2, 130.1, 127.6, 127.5, 127.0, 126.9, 125.8, 125.6, 125.1, 120.9, 118.5, 118.0, 115.0, 51.7, 42.2, 18.9. HRMS (ESI): calcd for $\text{C}_{25}\text{H}_{22}\text{O}_2\text{N}_5$ $[\text{M} + \text{H}]^+$ m/z 424.1768, found 424.1760; $\text{C}_{25}\text{H}_{21}\text{O}_2\text{N}_5\text{Na}$ $[\text{M} + \text{Na}]^+$ m/z 446.1588, found 446.1580.

Methyl 6-(4-((Pyridin-2-ylmethyl)amino)quinazolin-6-yl)imidazo[1,2-a]pyridine-2-carboxylate (10q)

Yellow solid, 53.8% yield, m.p. 143.7–145.6 °C. ^1H NMR (600 MHz, DMSO- d_6) δ 9.23 (s, 1H), 9.06 (s, 1H), 8.75 (s, 1H), 8.57 (s, 1H), 8.53 (d, $J = 4.8$ Hz, 1H), 8.48 (s, 1H), 8.16 (d, $J = 8.6$ Hz, 1H), 7.89 (d, $J = 9.5$ Hz, 1H), 7.83 (d, $J = 8.6$ Hz, 1H), 7.80 (d, $J = 9.5$ Hz, 1H), 7.74 (t, $J = 7.5$ Hz, 1H), 7.39 (d, $J = 7.8$ Hz, 1H), 7.29–7.25 (m, 1H), 4.92 (d, $J = 5.5$ Hz, 2H), 3.86 (s, 3H). ^{13}C NMR (150 MHz, DMSO) δ 163.0, 159.7, 158.4, 155.2, 149.0, 148.2, 143.9, 136.8, 135.9, 133.5, 131.0, 128.0, 126.7, 125.6, 125.1, 122.3, 121.2, 120.8, 118.5, 118.0, 115.1, 51.7, 45.8. HRMS (ESI): calcd for $\text{C}_{23}\text{H}_{19}\text{O}_2\text{N}_6$ $[\text{M} + \text{H}]^+$ m/z 411.1564, found 411.1556; $\text{C}_{23}\text{H}_{18}\text{O}_2\text{N}_6\text{Na}$ $[\text{M} + \text{Na}]^+$ m/z 433.1384, found 433.1372.

Methyl 6-(4-((2-Fluorobenzyl)amino)quinazolin-6-yl)imidazo[1,2-a]pyridine-2-carboxylate (10r)

Off-white solid, 52.1% yield, m.p. 174.0–176.2 °C. ^1H NMR (600 MHz, DMSO- d_6) δ 9.72 (s, 1H), 9.09 (s, 1H), 8.85 (s, 1H), 8.64 (s, 1H), 8.55 (s, 1H), 8.21 (s, 1H), 7.87 (t, $J = 11.8$ Hz, 2H), 7.76 (d, $J = 9.2$ Hz, 1H), 7.47 (t, $J = 7.6$ Hz, 1H), 7.33 (s, 1H), 7.22 (t, $J = 9.2$ Hz, 1H), 7.16 (t, $J = 7.4$ Hz, 1H), 4.92 (s, 2H), 3.85 (s, 3H). ^{13}C NMR (150 MHz, DMSO) δ 162.9, 161.1, 159.9, 159.4, 153.9, 143.8, 135.9, 134.3, 131.9, 129.7, 129.2, 126.6, 125.6, 125.3, 125.2, 124.4, 121.1, 118.5, 118.0, 115.3, 115.2, 114.5, 51.7, 38.1. ^{19}F NMR (565 MHz, DMSO) δ –118.44. HRMS (ESI): calcd for $\text{C}_{24}\text{H}_{19}\text{O}_2\text{N}_5\text{F}$ $[\text{M} + \text{H}]^+$ m/z 428.1517, found 428.1509; $\text{C}_{24}\text{H}_{18}\text{O}_2\text{N}_5\text{FNa}$ $[\text{M} + \text{Na}]^+$ m/z 450.1337, found 450.1330.

Methyl 6-(4-((3-Fluorophenyl)amino)quinazolin-6-yl)imidazo[1,2-a]pyridine-2-carboxylate (10s)

White solid, 48.6% yield, m.p. 179.3–181.6 °C. ^1H NMR (600 MHz, DMSO- d_6) δ 10.22–10.05 (m, 1H), 9.10 (s, 1H), 8.88 (s, 1H), 8.69 (s, 1H), 8.57 (s, 1H), 8.21 (dd, $J = 8.7, 2.0$ Hz, 1H), 7.97–7.88 (m, 3H), 7.81 (d, $J = 9.5$ Hz, 1H), 7.68 (d, $J = 8.1$ Hz, 1H), 7.49–7.41 (m, 1H), 6.98 (td, $J = 8.5, 2.6$ Hz, 1H), 3.86 (s, 3H). ^{13}C NMR (150 MHz, DMSO) δ 163.0, 162.8, 161.2, 157.7, 154.4, 148.8, 143.9, 140.8, 135.9, 134.3, 131.6, 130.1, 128.4, 126.9, 125.6, 125.4, 120.8, 118.5, 118.0, 115.3, 110.4, 109.2, 51.7. ^{19}F NMR (565 MHz, DMSO) δ –112.46. HRMS (ESI): calcd for $\text{C}_{23}\text{H}_{17}\text{O}_2\text{N}_5\text{F}$ $[\text{M} + \text{H}]^+$ m/z 414.1361, found 414.1347; $\text{C}_{23}\text{H}_{16}\text{O}_2\text{N}_5\text{FNa}$ $[\text{M} + \text{Na}]^+$ m/z 436.1180, found 436.1172.

Methyl 6-(4-(Methyl(p-tolyl)amino)quinazolin-6-yl)imidazo[1,2-a]pyridine-2-carboxylate (10t)

Pink flocculent, 39.5% yield, m.p. 172.8–174.3 °C. ¹H NMR (600 MHz, DMSO-*d*₆) δ 8.72 (s, 1H), 8.58 (s, 1H), 8.41 (s, 1H), 7.95 (dd, *J* = 8.7, 2.1 Hz, 1H), 7.83 (d, *J* = 8.6 Hz, 1H), 7.57 (d, *J* = 9.5 Hz, 1H), 7.36 (d, *J* = 8.0 Hz, 2H), 7.27 (d, *J* = 8.2 Hz, 2H), 7.06 (d, *J* = 2.1 Hz, 1H), 6.77 (dd, *J* = 9.5, 1.9 Hz, 1H), 3.85 (s, 3H), 3.57 (s, 3H), 2.41 (s, 3H). ¹³C NMR (150 MHz, DMSO) δ 162.9, 160.4, 154.4, 150.8, 145.1, 143.6, 137.0, 135.9, 131.8, 130.9 (2C), 130.2, 128.9, 126.4 (2C), 125.6, 125.3, 124.9, 124.0, 118.4, 117.8, 115.7, 51.7, 42.0, 20.6. HRMS (ESI): calcd for C₂₅H₂₂O₂N₅ [M + H]⁺ *m/z* 424.1768, found 424.1757; C₂₅H₂₁O₂N₅Na [M + Na]⁺ *m/z* 446.1588, found 446.1580.

Methyl 6-(4-(Ethyl(phenyl)amino)quinazolin-6-yl)imidazo[1,2-a]pyridine-2-carboxylate (10u)

Orange flocculent, 51.4% yield, m.p. 286.5–287.9 °C. ¹H NMR (600 MHz, DMSO-*d*₆) δ 8.73 (s, 1H), 8.38 (d, *J* = 9.2 Hz, 2H), 7.94 (d, *J* = 8.5 Hz, 1H), 7.84 (d, *J* = 8.6 Hz, 1H), 7.54 (d, *J* = 8.1 Hz, 3H), 7.46 (t, *J* = 7.4 Hz, 1H), 7.33 (d, *J* = 7.7 Hz, 2H), 7.20 (s, 1H), 6.98 (d, *J* = 8.7 Hz, 1H), 4.24 (q, *J* = 7.0 Hz, 2H), 3.88 (s, 3H), 1.31 (t, *J* = 6.9 Hz, 3H). ¹³C NMR (150 MHz, DMSO) δ 162.3, 159.8, 153.7 (2C), 150.7, 145.6, 143.2, 135.8, 131.5, 129.7 (2C), 129.6, 128.4, 126.4 (2C), 126.3, 125.2, 123.8, 123.4, 117.4, 117.2, 115.7, 50.7, 47.4, 11.4. HRMS (ESI): calcd for C₂₅H₂₂O₂N₅ [M + H]⁺ *m/z* 424.1768, found 424.1762; C₂₅H₂₁O₂N₅Na [M + Na]⁺ *m/z* 446.1588, found 446.1581.

4.1.3. General Experimental Protocol for Preparation of Compounds 13a–k**Procedure for the Preparation of 2-Phenyl-6-(4,4,5,5-tetramethyl-1,3,2-dioxaborolan-2-yl)imidazo[1,2-a]pyridine (12a)**

The components 5-(4,4,5,5-Tetramethyl-1,3,2-dioxaborolan-2-yl)pyridin-2-amine (1.2 g, 5.4 mmol), 2-bromoacetophenone **11a** (1.3 g, 6.5 mmol) and NaHCO₃ (1.4 g, 16 mmol) were added to EtOH (10 mL), and the mixture was heated to 80 °C and refluxed by condensation under argon for 4 h. After completion of the reaction (monitored by TLC), the solvent of the reaction mixture was removed under reduced pressure, and the mixture was extracted 2–3 times with ethyl acetate and saturated Na₂CO₃ solution. The organic phase was dried over anhydrous Na₂SO₄ and rotary dried under vacuum to form 2-phenyl-6-(4,4,5,5-tetramethyl-1,3,2-dioxaborolan-2-yl)imidazo[1,2-a]pyridine **12a** as pale-yellow oil substance (1.5 g, 4.7 mmol, 86.8% yield), ESI-MS: *m/z* 321.1 [M + H]⁺.

Compounds **12b–c** were synthesized according to the procedure described in **12a**. The ESI-MS information of compounds **12b–c** is listed as below:

Compound 2-(4-Fluorophenyl)-6-(4,4,5,5-tetramethyl-1,3,2-dioxaborolan-2-yl)imidazo[1,2-a]pyridine (12b)

Yellow solid, 81.5% yield, ESI-MS: *m/z* 337.2 [M + H]⁺.

Compound 2-Cyclopropyl-6-(4,4,5,5-tetramethyl-1,3,2-dioxaborolan-2-yl)imidazo[1,2-a]pyridine (12c)

Yellow solid, 81.5% yield, ESI-MS: *m/z* 283.2 [M + H]⁺.

Procedure for the Preparation of N-(2-fluorobenzyl)-6-(2-phenylimidazo[1,2-a]pyridin-6-yl)quinazolin-4-amine (13a)

N-(2-fluorobenzyl)-6-iodoquinazolin-4-amine **5i** (0.19 g, 0.5 mmol), 2-phenyl-6-(4,4,5,5-tetramethyl-1,3,2-dioxaborolan-2-yl)imidazo[1,2-a]pyridine **12a** (0.16 g, 0.5 mmol) and K₂CO₃ (0.21 g, 1.5 mmol) were added to 1,4-dioxane/water 10 mL [V_(1,4-dioxane):V_(water) = 4:1], and the mixture was heated to 100 °C under a protective atmosphere of argon followed by the addition of Pd(dppf)Cl₂. The mixture continues to be stirred under these conditions for a further 4–5 h. After completion of the reaction (monitored by TLC), the 1,4-dioxane and water were removed under reduced pressure, and the residue was purified through a column chromatography on silica with dichloromethane/methanol to afford N-(2-fluorobenzyl)-6-(2-phenylimidazo[1,2-a]pyridin-6-yl)quinazolin-4-amine **13a** as pink flocculent, 67.3% yield,

m.p. 130.8–132.2 °C. ^1H NMR (600 MHz, DMSO- d_6) δ 9.00 (s, 1H), 8.98 (t, J = 5.8 Hz, 1H), 8.72 (s, 1H), 8.50 (s, 1H), 8.44 (s, 1H), 8.18 (d, J = 8.7 Hz, 1H), 8.01 (d, J = 7.9 Hz, 2H), 7.82 (d, J = 8.6 Hz, 1H), 7.77 (q, J = 9.4 Hz, 2H), 7.46 (t, J = 7.6 Hz, 3H), 7.36–7.30 (m, 2H), 7.25–7.20 (m, 1H), 7.16 (t, J = 7.5 Hz, 1H), 4.88 (d, J = 5.5 Hz, 2H). ^{13}C NMR (150 MHz, DMSO) δ 161.2, 159.6, 159.5, 155.2, 148.7, 145.2, 144.2, 134.0, 133.8, 131.0, 129.6, 129.1, 128.8 (2C), 128.4, 127.9, 125.9, 125.8, 125.7 (2C), 125.1, 124.4, 120.3, 116.8, 115.3, 115.2, 109.7, 37.8. ^{19}F NMR (565 MHz, DMSO) δ –118.62. HRMS (ESI): calcd for $\text{C}_{28}\text{H}_{21}\text{N}_5\text{F}$ [$\text{M} + \text{H}$] $^+$ m/z 446.1776, found 446.1768.

Compounds **13b**–**13k** were synthesized according to the procedure described in **13a**. The information of compounds **13b**–**13k** is listed as below:

N-(2-fluorobenzyl)-6-(2-(4-fluorophenyl)imidazo[1,2-a]pyridin-6-yl)quinazolin-4-amine (**13b**)

Pink flocculent, 70.7% yield, m.p. 133.7–135.6 °C. ^1H NMR (600 MHz, DMSO- d_6) δ 9.00 (s, 1H), 8.96 (t, J = 5.4 Hz, 1H), 8.72 (s, 1H), 8.50 (s, 1H), 8.42 (s, 1H), 8.18 (d, J = 8.7 Hz, 1H), 8.04 (dd, J = 8.5, 5.5 Hz, 2H), 7.82 (d, J = 8.6 Hz, 1H), 7.79 (d, J = 9.4 Hz, 1H), 7.75 (d, J = 9.4 Hz, 1H), 7.45 (t, J = 7.7 Hz, 1H), 7.35–7.31 (m, 1H), 7.29 (t, J = 8.8 Hz, 2H), 7.24–7.20 (m, 1H), 7.16 (t, J = 7.5 Hz, 1H), 4.88 (d, J = 5.5 Hz, 2H). ^{13}C NMR (150 MHz, DMSO) δ 162.8, 161.1, 159.5, 155.2, 148.6, 144.2, 134.0, 131.0, 130.3, 129.6, 129.0, 128.3, 127.6, 125.9, 125.8, 125.1, 124.5, 124.4 (2C), 120.3, 116.7 (2C), 115.7, 115.6, 115.3, 115.2, 109.5, 37.7. ^{19}F NMR (565 MHz, DMSO) δ –113.19, –117.60. HRMS (ESI): calcd for $\text{C}_{28}\text{H}_{20}\text{N}_5\text{F}_2$ [$\text{M} + \text{H}$] $^+$ m/z 464.1681, found 464.1677.

N-(2,3-difluorophenyl)-6-(2-phenylimidazo[1,2-a]pyridin-6-yl)quinazolin-4-amine (**13c**)

Pink flocculent, 73.2% yield, m.p. 142.0–144.3 °C. ^1H NMR (600 MHz, DMSO- d_6) δ 10.22 (s, 1H), 9.08 (s, 1H), 8.86 (s, 1H), 8.56 (s, 1H), 8.46 (s, 1H), 8.28 (d, J = 8.4 Hz, 1H), 8.02 (d, J = 7.3 Hz, 2H), 7.93 (d, J = 8.7 Hz, 1H), 7.87–7.76 (m, 2H), 7.47 (t, J = 7.7 Hz, 2H), 7.40 (q, J = 8.6 Hz, 2H), 7.35 (t, J = 7.4 Hz, 1H), 7.30 (q, J = 7.2 Hz, 1H). ^{13}C NMR (150 MHz, DMSO) δ 158.5, 154.7, 151.3, 149.7, 149.6, 145.1, 144.2, 134.7, 133.6, 131.6, 129.7, 128.8 (2C), 128.4, 128.0, 125.7 (2C), 125.0, 124.7, 124.3, 124.3, 123.3, 120.7, 116.8, 115.1, 114.6, 109.7. ^{19}F NMR (565 MHz, DMSO) δ –137.37, –141.29. HRMS (ESI): calcd for $\text{C}_{27}\text{H}_{18}\text{N}_5\text{F}_2$ [$\text{M} + \text{H}$] $^+$ m/z 450.1525, found 450.1520; $\text{C}_{27}\text{H}_{17}\text{N}_5\text{F}_2\text{Na}$ [$\text{M} + \text{Na}$] $^+$ m/z 472.1344, found 472.1337.

N-(2,3-difluorophenyl)-6-(2-(4-fluorophenyl)imidazo[1,2-a]pyridin-6-yl)quinazolin-4-amine (**13d**)

Pink flocculent, 72.5% yield, m.p. 136.1–138.2 °C. ^1H NMR (600 MHz, DMSO- d_6) δ 10.21 (s, 1H), 9.07 (s, 1H), 8.85 (s, 1H), 8.56 (s, 1H), 8.43 (s, 1H), 8.28 (d, J = 8.8 Hz, 1H), 8.05 (dd, J = 8.5, 5.5 Hz, 2H), 7.92 (d, J = 8.7 Hz, 1H), 7.84 (d, J = 9.4 Hz, 1H), 7.78 (d, J = 9.4 Hz, 1H), 7.40 (q, J = 8.4 Hz, 2H), 7.29 (t, J = 8.7 Hz, 3H). ^{13}C NMR (150 MHz, DMSO) δ 162.8, 161.2, 158.4, 154.7, 151.2, 149.7, 144.2, 134.7, 131.6, 130.2, 128.4, 127.7 (2C), 127.6, 125.1, 124.7, 124.3, 124.2, 123.3, 120.6, 116.8, 115.7 (2C), 115.6, 115.1, 114.6, 109.6. ^{19}F NMR (565 MHz, DMSO) δ –113.15, –137.34, –141.32. HRMS (ESI): calcd for $\text{C}_{27}\text{H}_{17}\text{N}_5\text{F}_3$ [$\text{M} + \text{H}$] $^+$ m/z 468.1431, found 468.1426; $\text{C}_{27}\text{H}_{16}\text{N}_5\text{F}_3\text{Na}$ [$\text{M} + \text{Na}$] $^+$ m/z 490.1250, found 490.1239.

N-(cyclopropylmethyl)-6-(2-(4-fluorophenyl)imidazo[1,2-a]pyridin-6-yl)quinazolin-4-amine (**13e**)

Pink flocculent, 56.1% yield, m.p. 227.5–229.7 °C. ^1H NMR (600 MHz, DMSO- d_6) δ 8.99 (s, 1H), 8.64 (d, J = 2.2 Hz, 1H), 8.56 (t, J = 5.6 Hz, 1H), 8.48 (s, 1H), 8.43 (s, 1H), 8.18–8.11 (m, 1H), 8.05 (dd, J = 8.6, 5.6 Hz, 2H), 7.87–7.65 (m, 3H), 7.29 (t, J = 8.8 Hz, 2H), 3.46 (t, J = 6.1 Hz, 2H), 1.22 (td, J = 11.8, 4.7 Hz, 1H), 0.57–0.45 (m, 2H), 0.32 (q, J = 5.0 Hz, 2H). ^{13}C NMR (150 MHz, DMSO) δ 162.8, 161.1, 159.5, 155.4, 148.7, 144.2, 133.7, 130.7, 130.3, 128.3, 127.6 (2C), 125.2, 124.6, 124.3, 120.3, 116.7, 115.7 (2C), 115.2, 109.5, 45.2, 10.6, 3.6 (2C). ^{19}F NMR (565 MHz, DMSO) δ –114.24. HRMS (ESI): calcd for $\text{C}_{25}\text{H}_{21}\text{N}_5\text{F}$ [$\text{M} + \text{H}$] $^+$ m/z 410.1776, found 410.1773.

Compound 6-(2-phenylimidazo[1,2-a]pyridin-6-yl)-N-(1H-pyrazol-3-yl)quinazolin-4-amine (13f)

Pink solid, 54.6% yield, m.p. 289.1–290.1 °C. ¹H NMR (600 MHz, DMSO-*d*₆) δ 12.61 (s, 1H), 10.86 (s, 1H), 9.09 (s, 1H), 9.06 (s, 1H), 8.66 (s, 1H), 8.46 (s, 1H), 8.26 (d, *J* = 8.7 Hz, 1H), 8.03 (d, *J* = 7.6 Hz, 2H), 7.93 (d, *J* = 9.4 Hz, 1H), 7.88 (d, *J* = 8.6 Hz, 1H), 7.83–7.68 (m, 2H), 7.48 (t, *J* = 7.6 Hz, 2H), 7.36 (t, *J* = 7.3 Hz, 1H), 6.91 (s, 1H). ¹³C NMR (150 MHz, DMSO) δ 154.4, 149.4, 148.1, 145.0, 144.2, 134.4, 133.6, 131.2, 129.0, 128.8 (2C), 128.0, 127.8, 125.7 (2C), 125.2, 124.6, 124.3, 120.6, 116.6, 115.2, 109.7, 98.4. HRMS (ESI): calcd for C₂₄H₁₈N₇ [M + H]⁺ *m/z* 404.1618, found 404.1613; C₂₄H₁₇N₇Na [M + Na]⁺ *m/z* 426.1438, found 426.1426.

Compound 6-(2-cyclopropylimidazo[1,2-a]pyridin-6-yl)-N-(cyclopropylmethyl)quinazolin-4-amine (13g)

Yellow solid, 60.6% yield, m.p. 118.6–120.5 °C. ¹H NMR (600 MHz, DMSO-*d*₆) δ 8.89 (s, 1H), 8.60 (d, *J* = 2.1 Hz, 1H), 8.55 (t, *J* = 5.6 Hz, 1H), 8.46 (s, 1H), 8.09 (dd, *J* = 8.6, 2.0 Hz, 1H), 7.79 (s, 1H), 7.75 (d, *J* = 8.7 Hz, 1H), 7.68 (dd, *J* = 9.4, 1.9 Hz, 1H), 7.57 (d, *J* = 9.3 Hz, 1H), 3.45 (t, *J* = 6.2 Hz, 2H), 2.05 (ddd, *J* = 13.2, 8.3, 4.9 Hz, 1H), 1.25–1.18 (m, 1H), 0.92 (dt, *J* = 8.2, 2.9 Hz, 2H), 0.88–0.84 (m, 2H), 0.52–0.45 (m, 2H), 0.34–0.27 (m, 2H). ¹³C NMR (150 MHz, DMSO) δ 159.4, 155.2, 149.3, 148.5, 143.4, 134.0, 130.7, 128.2, 124.0, 123.8, 123.7, 120.1, 115.9, 115.2, 109.2, 45.2, 10.6, 9.5, 8.3 (2C), 3.6 (2C). HRMS (ESI): calcd for C₂₂H₂₂N₅ [M + H]⁺ *m/z* 356.1870, found 356.1863; C₂₂H₂₁N₅Na [M + Na]⁺ *m/z* 378.1690, found 378.1682.

Compound 6-(2-cyclopropylimidazo[1,2-a]pyridin-6-yl)-N-ethyl-N-phenylquinazolin-4-amine (13h)

Yellow solid, 58.3% yield, m.p. 166.8–168.7 °C. ¹H NMR (600 MHz, DMSO-*d*₆) δ 8.72 (s, 1H), 8.15 (s, 1H), 7.94 (dd, *J* = 8.7, 2.1 Hz, 1H), 7.80 (d, *J* = 8.6 Hz, 1H), 7.67 (s, 1H), 7.55 (t, *J* = 7.3 Hz, 2H), 7.53–7.50 (m, 1H), 7.34 (d, *J* = 7.5 Hz, 3H), 7.04 (d, *J* = 2.1 Hz, 1H), 6.76 (dd, *J* = 9.3, 1.9 Hz, 1H), 4.18 (q, *J* = 7.0 Hz, 2H), 1.99–2.05 (m, 1H), 1.23 (t, *J* = 7.0 Hz, 3H), 0.90 (dt, *J* = 8.2, 2.9 Hz, 2H), 0.85–0.81 (m, 2H). ¹³C NMR (150 MHz, DMSO) δ 160.0, 154.2, 150.8, 149.4, 145.9, 143.2, 132.6, 130.4 (2C), 130.4, 128.8, 127.2 (2C), 127.1, 123.5, 123.4, 123.3, 122.9, 115.8, 115.8, 109.1, 48.1, 11.7, 9.4, 8.2 (2C). HRMS (ESI): calcd for C₂₆H₂₄N₅ [M + H]⁺ *m/z* 406.2026, found 406.2019; C₂₆H₂₃N₅Na [M + Na]⁺ *m/z* 428.1846, found 428.1840.

N-ethyl-N-phenyl-6-(2-phenylimidazo[1,2-a]pyridin-6-yl)quinazolin-4-amine (13i)

Pink solid, 67.4% yield, m.p. 203.0–205.1 °C. ¹H NMR (600 MHz, DMSO-*d*₆) δ 8.74 (s, 1H), 8.32 (s, 1H), 8.26 (s, 1H), 8.03–7.97 (m, 3H), 7.83 (d, *J* = 8.6 Hz, 1H), 7.61–7.57 (m, 3H), 7.54 (d, *J* = 9.3 Hz, 1H), 7.45 (t, *J* = 7.6 Hz, 2H), 7.38 (dd, *J* = 6.8, 2.8 Hz, 2H), 7.34 (t, *J* = 7.3 Hz, 1H), 7.07 (d, *J* = 2.0 Hz, 1H), 6.87 (dd, *J* = 9.4, 1.9 Hz, 1H), 4.21 (q, *J* = 7.0 Hz, 2H), 1.25 (t, *J* = 7.0 Hz, 3H). ¹³C NMR (150 MHz, DMSO) δ 160.0, 154.1, 150.5, 145.8, 145.2, 143.9, 133.6, 132.4, 130.5 (2C), 128.7 (2C), 128.6, 127.9, 127.4, 127.2 (2C), 125.7 (2C), 124.3, 124.1, 123.9, 123.7, 116.6, 115.7, 109.5 (2C), 48.2, 11.7. HRMS (ESI): calcd for C₂₉H₂₄N₅ [M + H]⁺ *m/z* 442.2026, found 442.2021.

Compound 6-(2-phenylimidazo[1,2-a]pyridin-6-yl)-N-(pyridin-2-ylmethyl)quinazolin-4-amine (13j)

Pink solid, 70.2% yield, m.p. 141.9–143.3 °C. ¹H NMR (600 MHz, DMSO-*d*₆) δ 9.13 (t, *J* = 5.9 Hz, 1H), 9.02 (s, 1H), 8.75 (s, 1H), 8.54 (d, *J* = 4.3 Hz, 1H), 8.46 (s, 1H), 8.44 (s, 1H), 8.19 (dd, *J* = 8.7, 2.0 Hz, 1H), 8.01 (d, *J* = 7.5 Hz, 2H), 7.84–7.78 (m, 2H), 7.78–7.70 (m, 2H), 7.46 (t, *J* = 7.6 Hz, 2H), 7.39 (d, *J* = 7.9 Hz, 1H), 7.34 (t, *J* = 7.4 Hz, 1H), 7.29–7.25 (m, 1H), 4.93 (d, *J* = 5.8 Hz, 2H). ¹³C NMR (150 MHz, DMSO) δ 159.6, 158.6, 155.2, 149.0, 148.6, 145.2, 144.2, 136.8, 133.9, 133.7, 130.9, 128.8 (2C), 128.3, 127.9, 125.7 (2C), 125.0, 124.4, 124.4, 122.2, 121.2, 120.3, 116.8, 115.2, 109.7, 45.7. HRMS (ESI): calcd for C₂₇H₂₁N₆ [M + H]⁺ *m/z* 429.1822, found 429.1817.

Compound 6-(2-phenylimidazo[1,2-a]pyridin-6-yl)-N-((tetrahydro-2H-pyran-4-yl)methyl)quinazolin-4-amine (**13k**)

Pink solid, 69.8% yield, m.p. 127.0–129.3 °C. ¹H NMR (600 MHz, DMSO-*d*₆) δ 8.98 (s, 1H), 8.64 (s, 1H), 8.51 (t, *J* = 5.8 Hz, 1H), 8.49 (s, 1H), 8.44 (s, 1H), 8.14 (dd, *J* = 8.6, 2.0 Hz, 1H), 8.01 (d, *J* = 7.5 Hz, 2H), 7.80–7.74 (m, 3H), 7.46 (t, *J* = 7.6 Hz, 2H), 7.34 (t, *J* = 7.3 Hz, 1H), 3.86 (d, *J* = 11.2 Hz, 2H), 3.49 (t, *J* = 6.4 Hz, 2H), 3.28 (t, *J* = 11.0 Hz, 2H), 2.06–1.97 (m, 1H), 1.67 (d, *J* = 10.4 Hz, 2H), 1.32–1.24 (m, 2H). ¹³C NMR (150 MHz, DMSO) δ 159.7, 155.3, 148.5, 145.2, 144.2, 133.8, 133.8, 130.8, 128.8 (2C), 128.2, 127.9, 125.7 (2C), 125.1, 124.5, 124.3, 120.3, 116.8, 115.2, 109.7, 66.8 (2C), 46.3, 34.2, 30.7 (2C). HRMS (ESI): calcd for C₂₇H₂₆ON₅ [M + H]⁺ *m/z* 436.2132, found 436.2126.

4.2. Biological (Pharmacological) Research

4.2.1. Cell Culture

Human cell lines HCC827, A549, SH-SY5Y, HEL, MCF-7 and MRC-5 obtained from the Chinese Academy of Sciences Cell Bank (Shanghai, China) were treated with 10% foetal bovine serum (FBS, Biological Industries, Cromwell, CT, USA) and 1% antibiotics-antimycotics (100 units/mL penicillin G sodium, 100 µg/mL streptomycin, and 250 ng/mL amphotericin B) added to RPMI-1640 (HCC827, SH-SY5Y, HEL) or DMEM (A549, MCF-7, MRC-5) in culture. Cells were grown at 37 °C in an incubator containing water and 5% CO₂.

4.2.2. Antiproliferative Activity Assay

Cells were seeded in 96-well plates at 3000–5000 cells/well and treated with different concentrations of compounds for 72 h. After treatment, 20 µL MTT (Sigma-Aldrich, St. Louis, MO, USA) was added to each well, and incubation was continued in the incubator for 4 h. Purple formazan crystals were formed, the medium was discarded, 150 µL DMSO was added to dissolve the formazan, and the absorbance at 490 nm was measured by a multi-well spectrophotometer (Thermo Scientific, VARIOSKAN LUX, Waltham, MA, USA) to measure absorbance at 490 nm and to measure viability. IC₅₀ values were calculated based on the inhibition rate using GraphPad Prism software.

4.2.3. Molecular Modelling

Molecular docking simulations were performed using Molecular Operating Environment (MOE, Version 2020) [52]. PI3Kα (PDB code: 4ZOP) is selected for docking studies. Protein optimisation was performed by quickprep of the MOE. Docking sites were defined by the Site Finder program and Accelrys Discovery Studio Visualizer 4.5 was used for graphical display.

4.2.4. Kinase Assay

The inhibitory activity of compound **13k** against PI3Kα was determined using the ADP-Glo™ Max Assay, with HS-173 as a positive control, according to the kit instructions. Chemiluminescence values were measured by multi-well spectrophotometer (Thermo Scientific, VARIOSKAN LUX, USA).

4.2.5. Cell Cycle Assays

HCC827 cells were incubated in 6-well plates and treated with specific concentrations of **13k** for 48 h. Cells were collected and washed with PBS buffered solution, fixed overnight at –20 °C with pre-cooled 70% ethanol, supernatant discarded, washed with PBS buffered solution, stained by a mixture of propidium iodide (PI) and RNase, incubated for 30 min at room temperature protected from light and then detected using flow cytometry.

4.2.6. Hoechst 33342 Staining Assay

A portion of HCC827 cells were taken and inoculated overnight in 6-well plates and treated with different concentrations of compound **13k** for 48 h. Subsequent steps were carried

out according to the instructions of the Hoechst 33342 staining kit (Beyotime, Shanghai, China). Final pictures were taken with a microscope (DMi8, Leica, Wetzlar, Germany).

4.2.7. Apoptosis Assay

Apoptosis was detected by flow cytometry after staining with Annexin V-FITC and propidium iodide (PI) according to the manufacturer's protocol (BD Biosciences). HCC827 cells were inoculated overnight in 6-well plates, treated with specific concentrations of compound **13k** for 48 h. Cells were collected and incubated with 5 μ L of membrane linked protein V-FITC and 5 μ L of PI for 15–20 min protected from light, followed by flow cytometry analysis.

4.2.8. Western Blot Assay

Cells were treated with different concentrations of compound **13k** and then subjected to immunoblot analysis as described in a previous study. Blots were imaged by a ChemiDocTM MP imaging system (Bio-Rad, Hercules, CA, USA). All bands were analysed using Image J software. Antibodies were purchased from Cell Signaling Technology (CST, Danvers, MA, USA).

4.2.9. 3D Spheroid Cell Inhibition Assay

To culture HCC827 cancer cells into three-dimensional spheroids, we used PerkinElmer's CellCarrier Spheroid ULA 96-well microtiter plates (PerkinElmer, Waltham, MA, USA). In all experiments, cells were seeded at 40,000 cells per well. After spheroid formation, the spheroids were treated with **13k** at the indicated concentrations every 3 days. When significant changes in tumour spheroids were observed, photographs were taken using a ZEISS LSM 900 Airyscan 2 confocal laser scanning microscopy (ZEISS, Jena, Germany).

4.2.10. Statistical Analysis

All experimental data were replicated three times, and experimental results are expressed as mean \pm standard deviation (SD). Statistical analyses were manipulated and plotted using Photoshop, ImageJ, Graph Pad, etc., and tests were performed to assess statistically significant differences (* $p < 0.05$, ** $p < 0.01$, *** $p < 0.001$ or n.s. (not significant)).

Supplementary Materials: The following supporting information can be downloaded at: <https://www.mdpi.com/article/10.3390/ijms24076851/s1>.

Author Contributions: Conceptualization, M.L. and D.W.; Data curation, M.L. and D.W.; Formal analysis, Q.L., F.L. and T.Z.; Funding acquisition, Y.F.; Investigation, M.S.; Methodology, M.L. and D.W.; Project administration, Y.F.; Resources, Y.F.; Software, Q.L., F.L. and T.Z.; Supervision, Y.F.; Validation, H.W., L.X. and M.Y.; Visualization, M.L. and D.W.; Writing—original draft, M.L.; Writing—review and editing, M.L., D.W. and Y.F. All authors have read and agreed to the published version of the manuscript.

Funding: This work was supported by the National Natural Science Foundation of China (Grants 21907020 and 22167010), Merit-based Funding Program for Innovation and Entrepreneurship of High-level Overseas Talents of Guizhou Province (grant No. 202001), Natural Science Foundation of Guizhou Provincial Science and Technology Projects (QKH-zk [2022]030) and the Science and Technology Plan Project of Guizhou Province, China (QKHPTRC[2018]5779-58).

Institutional Review Board Statement: Not applicable for studies not involving humans or animals.

Informed Consent Statement: Not applicable.

Data Availability Statement: All data are included within the article and Supplementary Materials.

Acknowledgments: The authors wish to express their gratitude to their Analytical Testing Center for testing the NMR and HR-MS (ESI) data and to Ailing Linghu, Xinran Zhao of the Guizhou Medical University for helpful discussions on topics related to this work.

Conflicts of Interest: The authors declare that they have no known competing financial interests or personal relationships that could have appeared to influence the work reported in this paper.

References

1. Hernandez-Aya, L.F.; Gonzalez-Angulo, A.M. Targeting the phosphatidylinositol 3-kinase signaling pathway in breast cancer. *Oncologist* **2011**, *16*, 404–414. [[CrossRef](#)] [[PubMed](#)]
2. Thorpe, L.M.; Yuzugullu, H.; Zhao, J.J. PI3K in cancer: Divergent roles of isoforms, modes of activation and therapeutic targeting. *Nat. Rev. Cancer* **2015**, *15*, 7–24. [[CrossRef](#)] [[PubMed](#)]
3. Mayer, I.A.; Arteaga, C.L. The PI3K/AKT Pathway as a Target for Cancer Treatment. *Annu. Rev. Med.* **2016**, *67*, 11–28. [[CrossRef](#)] [[PubMed](#)]
4. Tewari, D.; Patni, P.; Bishayee, A.; Sah, A.N.; Bishayee, A. Natural products targeting the PI3K-Akt-mTOR signaling pathway in cancer: A novel therapeutic strategy. *Semin. Cancer Biol.* **2022**, *80*, 1–17. [[CrossRef](#)] [[PubMed](#)]
5. Yu, L.; Wei, J.; Liu, P. Attacking the PI3K/Akt/mTOR signaling pathway for targeted therapeutic treatment in human cancer. *Semin. Cancer Biol.* **2022**, *85*, 69–94. [[CrossRef](#)]
6. Wang, J.; Hu, K.; Cai, X.; Yang, B.; He, Q.; Wang, J.; Weng, Q. Targeting PI3K/AKT signaling for treatment of idiopathic pulmonary fibrosis. *Acta. Pharm. Sin. B* **2022**, *12*, 18–32. [[CrossRef](#)]
7. Zhang, M.; Jang, H.; Nussinov, R. PI3K inhibitors: Review and new strategies. *Chem. Sci.* **2020**, *11*, 5855–5865. [[CrossRef](#)] [[PubMed](#)]
8. Mazloumi Gavvani, F.; Smith Arnesen, V.; Jacobsen, R.G.; Krakstad, C.; Hoivik, E.A.; Lewis, A.E. Class I Phosphoinositide 3-Kinase PIK3CA/p110alpha and PIK3CB/p110beta Isoforms in Endometrial Cancer. *Int. J. Mol. Sci.* **2018**, *19*, 3931. [[CrossRef](#)]
9. Chen, W.; Dai, G.; Qian, Y.; Wen, L.; He, X.; Liu, H.; Gao, Y.; Tang, X.; Dong, B. PIK3CA mutation affects the proliferation of colorectal cancer cells through the PI3K-MEK/PDK1-GPT2 pathway. *Oncol. Rep.* **2022**, *47*, 11. [[CrossRef](#)]
10. Tserga, A.; Chatziandreou, I.; Michalopoulos, N.V.; Patsouris, E.; Saetta, A.A. Mutation of genes of the PI3K/AKT pathway in breast cancer supports their potential importance as biomarker for breast cancer aggressiveness. *Virchows. Arch.* **2016**, *469*, 35–43. [[CrossRef](#)]
11. Knowles, M.A.; Platt, F.M.; Ross, R.L.; Hurst, C.D. Phosphatidylinositol 3-kinase (PI3K) pathway activation in bladder cancer. *Cancer Metastasis Rev.* **2009**, *28*, 305–316. [[CrossRef](#)] [[PubMed](#)]
12. Sweetlove, M.; Wrightson, E.; Kolekar, S.; Rewcastle, G.W.; Baguley, B.C.; Shepherd, P.R.; Jamieson, S.M. Inhibitors of pan-PI3K Signaling Synergize with BRAF or MEK Inhibitors to Prevent BRAF-Mutant Melanoma Cell Growth. *Front. Oncol.* **2015**, *5*, 135. [[CrossRef](#)] [[PubMed](#)]
13. Vanhaesebroeck, B.; Perry, M.W.D.; Brown, J.R.; Andre, F.; Okkenhaug, K. Author Correction: PI3K inhibitors are finally coming of age. *Nat. Rev. Drug Discov.* **2021**, *20*, 798. [[CrossRef](#)]
14. Yang, J.; Nie, J.; Ma, X.; Wei, Y.; Peng, Y.; Wei, X. Targeting PI3K in cancer: Mechanisms and advances in clinical trials. *Mol. Cancer* **2019**, *18*, 26. [[CrossRef](#)]
15. Asif, M. Chemical characteristics, synthetic methods, and biological potential of quinazoline and quinazolinone derivatives. *Int. J. Med. Chem.* **2014**, *2014*, 395637. [[CrossRef](#)] [[PubMed](#)]
16. Dhuguru, J.; Ghoneim, O.A. Quinazoline Based HDAC Dual Inhibitors as Potential Anti-Cancer Agents. *Molecules* **2022**, *27*, 2294. [[CrossRef](#)]
17. Hameed, A.; Al-Rashida, M.; Uroos, M.; Ali, S.A.; Arshia; Ishtiaq, M.; Khan, K.M. Quinazoline and quinazolinone as important medicinal scaffolds: A comparative patent review (2011–2016). *Expert. Opin. Ther. Pat.* **2018**, *28*, 281–297. [[CrossRef](#)]
18. Ding, H.W.; Deng, C.L.; Li, D.D.; Liu, D.D.; Chai, S.M.; Wang, W.; Zhang, Y.; Chen, K.; Li, X.; Wang, J.; et al. Design, synthesis and biological evaluation of novel 4-aminoquinazolines as dual target inhibitors of EGFR-PI3Kalpha. *Eur. J. Med. Chem.* **2018**, *146*, 460–470. [[CrossRef](#)]
19. Teng, Y.; Li, X.; Ren, S.; Cheng, Y.; Xi, K.; Shen, H.; Ma, W.; Luo, G.; Xiang, H. Discovery of novel quinazoline derivatives as potent PI3Kdelta inhibitors with high selectivity. *Eur. J. Med. Chem.* **2020**, *208*, 112865. [[CrossRef](#)] [[PubMed](#)]
20. Zhou, Z.; He, J.; Yang, F.; Pan, Q.; Yang, Z.; Zheng, P.; Xu, S.; Zhu, W. Design, synthesis and evaluation of anti-proliferative activity of 2-aryl-4-aminoquinazoline derivatives as EGFR inhibitors. *Bioorg. Chem.* **2021**, *112*, 104848. [[CrossRef](#)]
21. Das, D.; Hong, J. Recent advancements of 4-aminoquinazoline derivatives as kinase inhibitors and their applications in medicinal chemistry. *Eur. J. Med. Chem.* **2019**, *170*, 55–72. [[CrossRef](#)] [[PubMed](#)]
22. Yadav, R.R.; Guru, S.K.; Joshi, P.; Mahajan, G.; Minto, M.J.; Kumar, V.; Bharate, S.S.; Mondhe, D.M.; Vishwakarma, R.A.; Bhushan, S.; et al. 6-Aryl substituted 4-(4-cyanomethyl) phenylamino quinazolines as a new class of isoform-selective PI3K-alpha inhibitors. *Eur. J. Med. Chem.* **2016**, *122*, 731–743. [[CrossRef](#)]
23. Fan, Y.H.; Ding, H.W.; Liu, D.D.; Song, H.R.; Xu, Y.N.; Wang, J. Novel 4-aminoquinazoline derivatives induce growth inhibition, cell cycle arrest and apoptosis via PI3Kalpha inhibition. *Bioorg. Med. Chem.* **2018**, *26*, 1675–1685. [[CrossRef](#)]
24. Altaher, A.M.; Adris, M.A.; Aliwaini, S.H.; Awadallah, A.M.; Morjan, R.Y. The Anticancer Effects of Novel Imidazo[1,2-a]Pyridine Compounds against HCC1937 Breast Cancer Cells. *Asian. Pac. J. Cancer Prev.* **2022**, *23*, 2943–2951. [[CrossRef](#)]
25. Dos Santos, D.C.; Rafique, J.; Saba, S.; Grinevicius, V.; Filho, D.W.; Zamoner, A.; Braga, A.L.; Pedrosa, R.C.; Ourique, F. IP-Se-06, a Selenylated Imidazo[1,2-a]pyridine, Modulates Intracellular Redox State and Causes Akt/mTOR/HIF-1alpha and MAPK Signaling Inhibition, Promoting Antiproliferative Effect and Apoptosis in Glioblastoma Cells. *Oxid. Med. Cell. Longev.* **2022**, *2022*, 3710449. [[CrossRef](#)] [[PubMed](#)]
26. Foki, E.; Stanisz, I.; Kadletz, L.; Kotowski, U.; Seemann, R.; Schmid, R.; Heiduschka, G. HS-173, a selective PI3K inhibitor, induces cell death in head and neck squamous cell carcinoma cell lines. *Wien. Klin. Wochenschr.* **2021**, *133*, 26–31. [[CrossRef](#)]
27. Hernandez-Prat, A.; Rodriguez-Vida, A.; Juanpere-Rodero, N.; Arpi, O.; Menendez, S.; Soria-Jimenez, L.; Martinez, A.; Iarchouk, N.; Rojo, F.; Albanell, J.; et al. Novel Oral mTORC1/2 Inhibitor TAK-228 Has Synergistic Antitumor Effects When Combined with Paclitaxel or PI3Kalpha Inhibitor TAK-117 in Preclinical Bladder Cancer Models. *Mol. Cancer Res.* **2019**, *17*, 1931–1944. [[CrossRef](#)] [[PubMed](#)]

28. Singh, D.; Yodun, T.; Kumar, G.; Ahmad Tali, J.; Tiwari, H.; Singh, J.; Nargotra, A.; Samykutty, A.; Singh, S.; Shankar, R. Synthesis of 3-N-/O-/S-methyl-imidazo[1,2-a] pyridine derivatives for caspase-3 mediated apoptosis induced anticancer activity. *Bioorg. Chem.* **2022**, *125*, 105882. [[CrossRef](#)]
29. Fan, Y.; Luo, F.; Su, M.; Li, Q.; Zhong, T.; Xiong, L.; Li, M.; Yuan, M.; Wang, D. Structure optimization, synthesis, and biological evaluation of 6-(2-amino-1H-benzo[d]imidazole-6-yl)-quinazolin-4(3H)-one derivatives as potential multi-targeted anticancer agents via Aurora A/ PI3K/BRD4 inhibition. *Bioorg. Chem.* **2023**, *132*, 106352. [[CrossRef](#)]
30. Li, P.; Lv, H.; Zhang, B.; Duan, R.; Zhang, X.; Lin, P.; Song, C.; Liu, Y. Growth Differentiation Factor 15 Protects SH-SY5Y Cells from Rotenone-Induced Toxicity by Suppressing Mitochondrial Apoptosis. *Front. Aging Neurosci.* **2022**, *14*, 869558. [[CrossRef](#)]
31. Niu, H.; Wang, D.; Wen, T.; Liu, H.; Jie, J.; Song, L.; Li, D. Anwuligan inhibits the progression of non-small cell lung cancer via let-7c-3p/PI3K/AKT/mTOR axis. *Cancer Med.* **2022**, *22*, 5382. [[CrossRef](#)]
32. Yadollahi-Farsani, M.; Amini-Farsani, Z.; Moayedi, F.; Khazaei, N.; Yaghoobi, H. MiR-548k suppresses apoptosis in breast cancer cells by affecting PTEN/PI3K/AKT signaling pathway. *IUBMB Life* **2023**, *75*, 97–116. [[CrossRef](#)]
33. Yang, Z.; Cai, W.; Chen, Y.; Guo, Z.; Xiao, Z.; Zhou, T.; Cheng, Y.; Xu, F. Jujuboside B Reverse CUMS-Promoted Tumor Progression via Blocking PI3K/Akt and MAPK/ERK and Dephosphorylating CREB Signaling. *J. Immunol. Res.* **2022**, *2022*, 5211368. [[CrossRef](#)]
34. Lien, E.C.; Dibble, C.C.; Toker, A. PI3K signaling in cancer: Beyond AKT. *Curr. Opin. Cell Biol.* **2017**, *45*, 62–71. [[CrossRef](#)] [[PubMed](#)]
35. Zhu, W.; Shi, L.; Gong, Y.; Zhuo, L.; Wang, S.; Chen, S.; Zhang, B.; Ke, B. Upregulation of ADAMDEC1 correlates with tumor progression and predicts poor prognosis in non-small cell lung cancer (NSCLC) via the PI3K/AKT pathway. *Thorac. Cancer* **2022**, *13*, 1027–1039. [[CrossRef](#)] [[PubMed](#)]
36. Jiang, L.; Zhang, J.; Xu, Y.; Xu, H.; Wang, M. Treating non-small cell lung cancer by targeting the PI3K signaling pathway. *Chin. Med. J. Engl.* **2022**, *135*, 1272–1284. [[CrossRef](#)]
37. Scheffler, M.; Bos, M.; Gardizi, M.; König, K. PIK3CA mutations in non-small cell lung cancer (NSCLC): Genetic heterogeneity, prognostic impact and incidence of prior malignancies. *Oncotarget* **2015**, *6*, 1315–1326. [[CrossRef](#)] [[PubMed](#)]
38. Tang, W.; Jia, P.; Zuo, L.; Zhao, J. Suppression of CX3CL1 by miR-497-5p inhibits cell growth and invasion through inactivating the ERK/AKT pathway in NSCLC cells. *Cell Cycle* **2022**, *21*, 1697–1709. [[CrossRef](#)] [[PubMed](#)]
39. Yan, Y.; Jin, X.; Sun, H.; Pang, S.; Kong, X.; Bu, J.; Xu, S. MiR-139-5p Targetedly Regulates YAF2 and Mediates the AKT/P38 MAPK Signaling Pathway to Alleviate the Metastasis of Non-Small Cell Lung Cancer Cells and Their Resistance against Cisplatin. *Cancer. Manag. Res.* **2021**, *13*, 3639–3650. [[CrossRef](#)] [[PubMed](#)]
40. Zheng, B.; Zheng, Y.; Zhang, N.; Zhang, Y.; Zheng, B. Rhoifolin from Plumula Nelumbinis exhibits anti-cancer effects in pancreatic cancer via AKT/JNK signaling pathways. *Sci. Rep.* **2022**, *12*, 5654. [[CrossRef](#)]
41. Rovida, E.; Tusa, I. Targeting MAPK in Cancer 2.0. *Int. J. Mol. Sci.* **2022**, *23*, 5702. [[CrossRef](#)]
42. Mansour, M.A.; Lasheen, D.S.; Gaber, H.M.; Abouzid, K.A.M. Elaborating piperazinyl-fuopyrimidine based scaffolds as phosphoinositol-3-kinase enzyme alpha (PI3Kalpha) inhibitors to combat pancreatic cancer. *RSC Adv.* **2020**, *10*, 32103–32112. [[CrossRef](#)] [[PubMed](#)]
43. Koledova, Z. 3D Cell Culture: An Introduction. *Methods. Mol. Biol.* **2017**, *1612*, 1–11. [[CrossRef](#)] [[PubMed](#)]
44. Langhans, S.A. Using 3D in vitro cell culture models in anti-cancer drug discovery. *Expert Opin. Drug Discov.* **2021**, *16*, 841–850. [[CrossRef](#)] [[PubMed](#)]
45. Ravi, M.; Paramesh, V.; Kaviya, S.; Anuradha, E.; Solomon, F. 3D cell culture systems: Advantages and applications. *J. Cell. Physiol.* **2015**, *230*, 16–26. [[CrossRef](#)] [[PubMed](#)]
46. Gu, C.; Feng, J.; Waqas, A.; Deng, Y.; Zhang, Y.; Chen, W.; Long, J.; Huang, S.; Chen, L. Technological Advances of 3D Scaffold-Based Stem Cell/Exosome Therapy in Tissues and Organs. *Front. Cell Dev. Biol.* **2021**, *9*, 709204. [[CrossRef](#)]
47. Pashuck, E.T.; Stevens, M. From clinical imaging to implantation of 3D printed tissues. *Nat. Biotechnol.* **2016**, *34*, 295–296. [[CrossRef](#)]
48. Wang, J.; Zhang, X.; Li, X.; Zhang, Y.; Hou, T.; Wei, L.; Qu, L.; Shi, L.; Liu, Y.; Zou, L.; et al. Anti-gastric cancer activity in three-dimensional tumor spheroids of bufadienolides. *Sci. Rep.* **2016**, *6*, 24772. [[CrossRef](#)]
49. Kniebs, C.; Luengen, A.E.; Guenther, D.; Cornelissen, C.G.; Schmitz-Rode, T.; Jockenhoevel, S.; Thiebes, A.L. Establishment of a Pre-vascularized 3D Lung Cancer Model in Fibrin Gel-Influence of Hypoxia and Cancer-Specific Therapeutics. *Front. Bioeng. Biotechnol.* **2021**, *9*, 761846. [[CrossRef](#)]
50. Han, K.; Pierce, S.E.; Li, A.; Spees, K.; Anderson, G.R.; Seoane, J.A.; Lo, Y.H.; Dubreuil, M.; Olivas, M.; Kamber, R.A.; et al. CRISPR screens in cancer spheroids identify 3D growth-specific vulnerabilities. *Nature* **2020**, *580*, 136–141. [[CrossRef](#)]
51. Xiao, Z.; Osipyanyan, A.; Song, S.; Chen, D.; Schut, R.A.; van Merkerk, R.; van der Wouden, P.E.; Cool, R.H.; Quax, W.J.; Melgert, B.N.; et al. Thieno[2,3-d]pyrimidine-2,4(1H,3H)-dione Derivative Inhibits d-Dopachrome Tautomerase Activity and Suppresses the Proliferation of Non-Small Cell Lung Cancer Cells. *J. Med. Chem.* **2022**, *65*, 2059–2077. [[CrossRef](#)] [[PubMed](#)]
52. Yang, H.; Li, Q.; Su, M.; Luo, F.; Liu, Y.; Wang, D.; Fan, Y. Design, synthesis, and biological evaluation of novel 6-(pyridin-3-yl) quinazolin-4(3H)-one derivatives as potential anticancer agents via PI3K inhibition. *Bioorg. Med. Chem.* **2021**, *46*, 116346. [[CrossRef](#)] [[PubMed](#)]

Disclaimer/Publisher's Note: The statements, opinions and data contained in all publications are solely those of the individual author(s) and contributor(s) and not of MDPI and/or the editor(s). MDPI and/or the editor(s) disclaim responsibility for any injury to people or property resulting from any ideas, methods, instructions or products referred to in the content.